



HAL
open science

Hepatitis B virus targets lipid transport pathways to infect hepatocytes

Knud Esser, Xiaoming Cheng, Jochen Wettengel, Julie Lucifora, Lea Hansen-Palmus, Katharina Austen, Armando A.R. Suarez, Sarah Heintz, Barbara Testoni, Firat Nebioglu, et al.

► **To cite this version:**

Knud Esser, Xiaoming Cheng, Jochen Wettengel, Julie Lucifora, Lea Hansen-Palmus, et al.. Hepatitis B virus targets lipid transport pathways to infect hepatocytes. Cellular and Molecular Gastroenterology and Hepatology, In press, 10.1016/j.jcmgh.2023.03.011 . hal-04069375

HAL Id: hal-04069375

<https://hal.science/hal-04069375>

Submitted on 14 Apr 2023

HAL is a multi-disciplinary open access archive for the deposit and dissemination of scientific research documents, whether they are published or not. The documents may come from teaching and research institutions in France or abroad, or from public or private research centers.

L'archive ouverte pluridisciplinaire **HAL**, est destinée au dépôt et à la diffusion de documents scientifiques de niveau recherche, publiés ou non, émanant des établissements d'enseignement et de recherche français ou étrangers, des laboratoires publics ou privés.

Hepatitis B virus targets lipid transport pathways to infect hepatocytes

Knud Esser^{*1}, Xiaoming Cheng^{*1}, Jochen M. Wettengel^{*1}, Julie Lucifora^{2,3}, Lea Hansen-Palmus¹, Katharina Austen¹, Armando A. R. Suarez³, Sarah Heintz³, Barbara Testoni³, Firat Nebioglu⁴, Minh Tu Pham⁴, Shangqing Yang⁴, Alma Zerneck⁵, Dirk Wohlleber^{6,7}, Marc Ringelhan^{7,8}, Mathias Broxtermann¹, Daniel Hartmann⁹, Norbert Hüser⁹, Julia Mergner¹⁰, Andreas Pichlmair^{1,7,10}, Wolfgang E. Thasler¹¹, Mathias Heikenwalder¹, Georg Gasteiger¹, Andreas Blutke¹², Axel Walch¹², Percy A. Knolle^{6,7}, Ralf Bartenschlager^{4,7,13} and Ulrike Protzer^{1,7}

*Authors contributed equally to the work

¹Institute of Virology, Technical University of Munich, School of Medicine / Helmholtz Munich, Trogerstr. 30, 81675 Munich, Germany

²INSERM U1052, CNRS UMR-5286, Cancer Research Center of Lyon (CRCL), Lyon, France. University of Lyon, Université Claude-Bernard (UCBL), Lyon, France.

³CIRI—Centre International de Recherche en Infectiologie, Inserm, U1111, Univ Lyon, Université Claude Bernard Lyon 1, CNRS, UMR5308, ENS Lyon

⁴Heidelberg University, Medical Faculty Heidelberg, Department of Infectious Diseases, Molecular Virology, Center for Integrative Infectious Diseases Research, Im Neuenheimer Feld 344, 69120 Heidelberg, Germany

⁵Institute of Experimental Biomedicine, University Hospital Würzburg, Josef-Schneider-Str. 2, Würzburg 97080, Germany

⁶Institute of Molecular Immunology and Experimental Oncology, University Hospital rechts der Isar, Technical University of Munich, School of Medicine, Ismaninger Str. 22, 81675 Munich, Germany

⁷German Center for Infection Research (DZIF), Munich and Heidelberg partner sites

⁸2nd Medical Department, University Hospital rechts der Isar, Technical University of Munich, School of Medicine, Ismaninger Str. 22, 81675 Munich, Germany

⁹Department of Surgery, University Hospital rechts der Isar, Technical University of Munich, School of Medicine, Ismaninger Str. 22, 81675 Munich Germany

¹⁰Bavarian Center for Biomolecular Mass Spectrometry at Klinikum rechts der Isar (BayBioMS@MRI), TUM, Munich, Germany

34 ¹¹Department of General, Visceral, Transplantation, Vascular and Thoracic Surgery, Grosshadern
35 Hospital, Ludwig Maximilians University, Nussbaumstr. 20, 80336 Munich, Germany

36 ¹²Institute of Pathology, Helmholtz Zentrum München, Ingolstädter Landstr. 1, 85764 Neuherberg,
37 Germany

38 ¹³Division Virus-Associated Carcinogenesis, German Cancer Research Center (DKFZ), Im
39 Neuenheimer Feld 280, 69120 Heidelberg, Germany

40

41 **Short Title:** HBV targets the cholesterol transport

42 **Author Contributions:** Study concept and design: KE, XC, PAK, RB, UP; Acquisition of
43 data: KE, XC, JL, LHP, KA, DW, MR, JMW, FM, MTP, SY, MB, AB;
44 Analysis and interpretation of data: KE, XC, JL, JMW, DW, MR, MG, KA,
45 MH, GG, AW, PAK, UP; Administrative, technical, or material support:
46 DH, NH, AZ, WET; Obtained funding: MH, PAK, RB, UP; Drafting of the
47 manuscript: KE, XC, PAK, UP; Critical revision of the manuscript for
48 important intellectual content: all authors.

49 **Grant support:** This study was supported by grants from the Deutsche
50 Forschungsgemeinschaft (project number 272983813 – TRR 179),
51 projects TP 05 to PK, TP 06 to MH, TP09 to RB, TP11 to AP and TP 14
52 to UP, the German Center for Infection Research (DZIF) project 05.806
53 and by the European Union's Horizon 2020 research and innovation
54 programme under grant agreement 848223 (VIROFIGHT consortium).
55 BT, AARS and SH were supported by public grants overseen by the
56 French National Research Agency (ANR) as part of the second
57 "Investissements d'Avenir" program (reference: ANR-17-RHUS-0003)
58 and by the European Union (grant EU H2020-847939-IP-cure-B).

59 **Correspondence:** Knud Esser, PhD and Prof. Ulrike Protzer, MD
60 Institute of Virology, TUM / Helmholtz Zentrum München
61 Trogerstr. 30, D-81675 Munich, Germany
62 protzer@tum.de; protzer@helmholtz-muenchen.de; knud.esser@tum.de
63 +49 89 4140 6821; +49 211 810 6025

64 **Disclosure:** The authors declare no conflict of interest relevant to this manuscript
65 and the data reported

66 **Word Count:** summary: 241 words; synopsis: 39 words;
67 main document text: 4367 words; 40 references

68 **Writing assistance:** None

69 **Data transparency:** all data, analytical methods and study materials will be made available to
70 other researchers upon reasonable request to the corresponding author

71 **Abbreviations:** Apo: apolipoprotein
72 BODIPY: dipyrrometheneboron difluoride
73 cccDNA: covalently closed circular DNA
74 CMFDA: chloromethylfluorescein diacetate
75 DNA: deoxyribonucleic acid
76 DC-SIGN: dendritic cell-specific intercellular adhesion molecule-3-
77 grabbing nonintegrin
78 HBeAg: HBV e antigen
79 HBsAg: HBV surface antigen
80 HBV: Hepatitis B virus
81 HDL: high density lipoprotein
82 HSPG: heparan sulfate proteoglycan
83 IDL: intermediate density lipoprotein
84 LAMP 1: lysosomal-associated membrane protein 1
85 LDL: low density lipoprotein
86 LRP: LDL-receptor related protein
87 LSEC: liver sinusoidal endothelial cells
88 L-SIGN: liver/lymph node-specific intercellular adhesion molecule-3-
89 grabbing nonintegrin
90 NBD: nitrobenzoxadiazole
91 NPC-1: Niemann-Pick C1
92 NTCP: sodium taurocholate cotransporting polypeptide
93 Rab 11: Ras-related protein Rab-11A
94 TG: triglyceride
95 VLDL: very low density lipoprotein
96 VP: viral particle
97

98 **Synopsis (40 words):**

99 A single HBV virion suffices to infect an individual indicating that it hijacks a physiological
100 pathway targeting hepatocytes. HBV associates with lipoproteins to access the perisinusoidal
101 space or to follow the physiological cholesterol transport pathway to hepatocytes via
102 macrophages.

103

104 **Graphical Abstract: Model for HBV host cell targeting to achieve hepatocyte infection.**

105

106

107 ApoE: apolipoprotein E; ApoA1: apolipoprotein A1; EE: early endosome; HSPG: heparan sulfate
108 proteoglycans; KC: liver macrophages (Kupffer cell); LDL-R: LDL-receptor; LE: late endosome; LSEC:
109 liver sinusoidal endothelial cell; Lys: lysosome; NPC1: Niemann Pick Typ C 1 protein; NTCP: sodium
110 taurocholate cotransporting polypeptide; RE: recycling endosome; SC: Stellate cell; TRL: triglyceride-
111 rich lipoprotein remnant

112 **Abstract (260 words)**

113 **Background and aims:** A single hepatitis B virus (HBV) particle is sufficient to establish
114 chronic infection of the liver after intravenous injection, suggesting that the virus targets
115 hepatocytes via a highly efficient transport pathway. We therefore investigated whether HBV
116 utilizes a physiological liver-directed pathway that supports specific host-cell targeting *in vivo*.

117 **Methods:** We established an *ex vivo* system of perfused human liver tissue that recapitulates
118 the liver physiology to investigate HBV liver targeting. This model allowed us to investigate
119 virus-host cell interactions in a cellular microenvironment mimicking the *in vivo* situation.

120 **Results:** HBV was rapidly sequestered by liver macrophages within one hour after a virus
121 pulse, but was detected in hepatocytes only after 16 hours. We found that HBV associates
122 with lipoproteins. Electron- and immunofluorescence microscopy corroborated a co-
123 localization in recycling endosomes within peripheral and liver macrophages. Importantly,
124 recycling endosomes accumulated HBV and cholesterol, followed by transport of HBV back to
125 the cell surface along the cholesterol efflux pathway. To reach hepatocytes as final target cells,
126 HBV was able to utilise the hepatocyte-directed cholesterol transport machinery of
127 macrophages.

128 **Conclusions:** Our results propose that HBV by binding to liver targeted lipoproteins and
129 utilizing the reverse cholesterol transport pathway of macrophages hijacks the physiological
130 lipid transport pathways to the liver to most efficiently reach its target organ. This may involve
131 trans-infection of liver macrophages and result in deposition of HBV in the perisinusoidal space
132 from where HBV can bind its receptor on hepatocytes.

133

134 **Keywords**

135 Transcytosis, trans-infection, liver targeting, lipoprotein metabolism

136

137 **Introduction**

138 Hepatitis B virus (HBV) belongs to the family hepadnaviridae and is a highly infectious and
139 organ specific pathogen. Currently over 290 million humans worldwide are chronically infected
140 with HBV and at high risk to develop liver cirrhosis or hepatocellular carcinoma
141 (www.who.int/mediacentre/factsheets/fs204/en/). The successful dissemination of HBV within
142 the human population relies mainly on vertical transmission that allows an immune escape of
143 the virus or sexual transmission that requires an efficient transmission at a low infection dose.
144 HBV infectivity indeed is extraordinarily high, and during experimental infection in
145 chimpanzees, a single virion was reported to suffice to establish HBV infection¹. Recently, the
146 sodium taurocholate cotransporting polypeptide (NTCP) expressed on the basolateral
147 membrane i.e. side of hepatocytes facing the liver sinusoid has been identified as a crucial
148 receptor². Following initial attachment of HBV virion to heparan sulfate proteoglycans
149 (HSPG)^{3,4}, that are typically found in the space of Dissé between liver sinusoidal endothelial
150 cells and hepatocytes, NTCP binds the myristoylated N-terminal part of the large HBV surface
151 protein. How HBV can gain access to the liver and to its receptor on the hepatocyte so
152 efficiently, however, is not understood.

153 In the liver, hepatocytes are lined and shielded from pathogens and gut-derived toxins by a
154 layer of fenestrated liver sinusoidal endothelial cells (LSEC), on top of which Kupffer cells are
155 located representing the largest population of organ-resident macrophages in the body. For
156 some hepatotropic pathogens there is evidence that sinusoidal liver cells contribute to
157 hepatocyte infection⁵. Hepatitis C virus (HCV) has been shown to be captured by the C-type
158 lectin dendritic cell-specific intercellular adhesion molecule-3-grabbing nonintegrin (DC-SIGN)
159 and a liver/lymph node-specific version (L-SIGN)⁶, that both are present on LSEC⁷. Cells
160 expressing DC-SIGN and L-SIGN can trans-infect hepatocytes with HCV⁸ and LSEC can
161 promote HCV infection in a paracrine fashion⁹. The duck analogue of HBV was reported to be
162 taken up preferentially by LSEC and not by hepatocytes *in vivo*¹⁰ suggesting that LSEC remove
163 duck HBV from the circulation and subsequently deliver it to hepatocytes.

164 For plasmodium sporozoites, intravital microscopy of mouse liver showed sporozoite
165 transmigration through Kupffer cells and LSEC escaping lysosomal compartments before
166 entering hepatocytes^{11,12}. Thus, there is evidence that pathogens may exploit trans-cellular
167 transport processes to target hepatocytes in a similar fashion as molecules like transferrin or
168 ceruloplasmin transporting iron and copper, respectively. We recently showed that HBV
169 infection of hepatocytes is significantly reduced when lipases are inhibited, and found a
170 reduced hepatic virus uptake *in vivo* if apolipoprotein (Apo) E is lacking¹³. These data are in
171 line with the finding that ApoE-specific antibodies inhibit HBV infection¹⁴. This indicated a
172 transport pathway employed by HBV along with lipoproteins to efficiently target hepatocytes.

173 The liver plays a key role in lipid metabolism. It takes up and oxidizes triglycerides (TG),
174 converts excess carbohydrates and proteins into fatty acids and TG to provide energy and
175 synthesizes cholesterol, phospholipids and Apo. Furthermore, it secretes cholesterol into bile
176 or converts it to bile salts. TG and cholesterol are hydrophobic neutral lipids that travel within
177 the water-based blood embedded within lipoprotein particles containing Apo. Lipoprotein
178 particles are divided by their density relative to surrounding water into ultra-low density
179 chylomicrons, very low (VLDL), intermediate (IDL), low (LDL) and high (HDL) density
180 lipoproteins.

181 Ultra-low density chylomicrons transport lipids absorbed from the intestine to adipose, cardiac,
182 and skeletal muscle tissue, where their TG components are hydrolyzed by lipoprotein lipases
183 and released. When most of the TG have been hydrolyzed, the chylomicron remnants become
184 enriched with ApoE and ApoC2, the coenzyme for lipoprotein lipase, and are taken up by
185 hepatocytes where remaining neutral lipids become hydrolyzed by cellular lipases¹⁵. VLDL are
186 assembled within hepatocytes and released into the blood stream to transport “endogenous”
187 TG, phospholipids and cholesterol. VLDL release TG and become IDL and then LDL with ApoE
188 determining their recycling to the liver. HDL particles remove cholesterol and fatty acids from
189 cells and exchange neutral lipids with VLDL. ApoE is also present in a subfraction of HDL,
190 HDL_E, where it serves as a major factor determining their rapid uptake into the liver¹⁶.

191 There is strong evidence that in case of postprandial lipoprotein peaks or hyperlipoproteinemia
192 Kupffer cells contribute to hepatic clearance of circulating lipoprotein, either due to higher
193 average lipoprotein size or due to oxidative modification¹⁷. Once lipoproteins have passed the
194 endothelial cell layer and reach the space of Disse, they are trapped by electrostatic
195 interactions with HSPG. There, hepatic lipase remodels the particles, giving them an optimal
196 size to interact with cell surface receptors and ApoE. The receptors that bind and take up
197 ApoE-containing remnant particles include the LDL receptor, the LDL-receptor related protein
198 (LRP)-1 and HSPG¹⁸. Additionally, excess cholesterol is transported back to the liver in a
199 process known as reverse cholesterol transport mainly via high density lipoprotein (HDL). From
200 lipoproteins initially taken up by macrophages cholesterol can be effluxed to HDL and
201 transported to the liver. Within macrophages, cholesterol esters of endocytosed lipoproteins
202 become hydrolysed by the endosomal acid lipase before free cholesterol is transported to the
203 cell membrane via a Niemann-Pick C1 (NPC1)-dependent mechanism¹⁵. Finally, free
204 cholesterol is released from the macrophage and can bind extracellular lipid receptors such as
205 HDL enabling uptake into hepatocytes. Little is known about how much liver macrophages
206 contribute to reverse cholesterol transport to hepatocytes.

207 Since only humans or primates are productively infected with HBV and small animal models
208 are lacking, we developed a novel infection model system, in which human liver tissue is
209 perfused with labelled viral particles (VP). Using this *ex vivo* liver perfusion model we
210 unexpectedly found that HBV in association with lipoproteins was preferentially taken up by
211 liver macrophages into recycling endosomes and only thereafter accumulated in hepatocytes.
212 Macrophages re-secreted HBV in association with free cholesterol derived from endocytosed
213 lipoproteins. Finally, HBV was taken up by hepatocytes along with macrophage-derived neutral
214 lipids supporting the conclusion that HBV can exploit the macrophage cholesterol transport as
215 one way to reach its host cell, the hepatocyte. We thus hypothesize that HBV uptake into
216 macrophages and subsequent trans-infection of hepatocytes represents an efficient strategy
217 for the pathogen to be sequestered in the liver, to avoid scavenger cells in the circulation or
218 spleen and to target hepatocytes.

219 **Results**

220 **HBV primarily associates with liver macrophages prior to infecting hepatocytes**

221 To identify the cell populations in the liver that in a physiological fashion are rapidly associated
222 with HBV, we established an *ex vivo* human liver tissue perfusion model with medium and
223 human serum (**Fig 1A**). Tissue viability was confirmed after 17-hour perfusion by scavenger
224 receptor-mediated uptake of ovalbumin into liver sinusoidal endothelial cells (**Fig 1B**). To
225 visualise early HBV infection events, we used purified viral particles (VP) comprising a mixture
226 of virions and filamentous subviral particles that express all three HBV envelope proteins (S,
227 M and L), and labelled them with Alexa594 fluorochrome (VP₅₉₄) (**Fig 1C**). Such HBV VP₅₉₄
228 were added to isolated liver macrophages and uptake of VP was detected and confirmed by
229 HBs staining using polyclonal antibodies. This demonstrated that purification and labelling
230 neither affected HBV envelope protein integrity nor particle uptake (**Fig 1D**). Co-localisation of
231 VP₅₉₄ with HBsAg-specific staining confirmed specificity of VP₅₉₄-fluorescence labelling.
232 Staining of HBs after *ex vivo* perfusion of human liver tissue with HBV VP indicated uptake into
233 sinusoidal lining cells (**Fig 1E**). Antibody staining specificity was confirmed by absence of
234 staining of HBV-negative liver tissue (**Fig 1F**).

235 To study the physiological interaction of HBV with liver cells in the presence of serum
236 components the perfusion medium was supplemented with 50% human serum collected during
237 a postprandial phase from a HBV-naïve and non-vaccinated individual. Demonstrating a
238 productive infection of hepatocytes by HBV in this experimental system, we detected HBV
239 cccDNA, the nuclear transcription template of HBV, at three days after the perfusion with HBV
240 particles, and secretion of newly synthesized HBV e antigen (HBeAg) (**Fig 2A**). Strikingly, after
241 a 45 min perfusion of the liver tissue with VP₅₉₄ in medium containing human serum,
242 quantitative immunofluorescence analysis revealed that 97±2 % of CD68-positive liver
243 macrophages but not (0.9±1.3%) CD68-negative cells such as hepatocytes had taken up VP₅₉₄
244 (**Fig 2B-D**). Similar results were obtained following perfusion of human liver tissue with
245 unlabelled HBV and detection of viral particles by immunofluorescence staining (**Fig 2E**).

246 Notably, HBV particles were also detected in liver macrophages in tissue sections from HBV-
247 infected patients (**Fig 2F**). Moreover, a localization to macrophages was confirmed *in vivo*
248 when we injected VP or HBV purified from human plasma into mice. Within 45 minutes or 1 h
249 after intravenous injection, respectively, liver macrophages had already accumulated
250 fluorescently labelled VP₅₉₄ and HBV DNA (**Fig 2G-I**). Taken together, these data indicate that
251 HBV rapidly accumulates in macrophages but not hepatocytes thus raising the question
252 whether HBV can escape lysosomal degradation in macrophages.

253

254 **HBV localizes to recycling endosomes within macrophages**

255 Since macrophages are specialised to clear pathogens from the circulation by lysosomal
256 degradation, we next defined the intracellular location of internalized HBV particles in liver
257 macrophages. To proof endocytosis of infectious HBV by human liver macrophages, isolated
258 liver macrophages were incubated with purified HBV at 4°C or 37°C, respectively, and cellular
259 viral rcDNA content was quantified. A significant increase of HBV rcDNA was detected
260 associated with cells incubated at 37°C illustrating that liver macrophages do not only bind but
261 actively take up infectious HBV (**Fig 3A**).

262 To determine the exact intracellular localization within liver macrophages, immunostainings
263 and confocal microscopy were performed. Already after one hour, VP₅₉₄ accumulated in an
264 LAMP1-negative but Rab11-positive endosome, indicative of recycling endosomes but not
265 lysosomes (**Fig 3B,C**). Even after 17h, HBV particles remained localized in LAMP1-negative,
266 Rab11-positive recycling endosomes (**Fig 3D,E**). The localization of VP₅₉₄ to recycling
267 endosomes was confirmed using macrophages differentiated from the monocyte-macrophage
268 cell line THP (**Fig 4A,B,D,F**). In striking contrast, recombinant subviral particles containing only
269 HBV S but lacking L and M proteins concentrated selectively in lysosomes (**Fig 4C,E,G**).

270 These data suggest that viral particles containing the L protein but not subviral particles without
271 escape lysosomal trafficking and degradation within macrophages by targeting vesicles that
272 are involved in recycling of endocytosed molecules to the cell surface.

273

274 **HBV associates with lipoproteins in cell culture, in blood and in macrophages**

275 We next addressed the question, which transport pathway within macrophages was hijacked
276 by HBV to escape lysosomal degradation in perfused human liver tissue. Ultrastructural
277 analysis found HBV particles accumulated in liver macrophages (**Fig 5A**). These were virions
278 fulfilling all ultrastructural characteristics reported¹⁹ and, to a lesser extend, filamentous
279 subviral particles. No such particles were detected in non-perfused liver tissue. Within the
280 macrophage, HBV was membrane-associated within intracellular, perinuclear compartments
281 or small vesicles. Interestingly, HBV-positive vesicles also contained lipoproteins, which
282 according to their size (70 nm) were most likely ultra-low density chylomicrons or VLDL (**Fig**
283 **5A**).

284 This prompted us to study whether HBV is associated with lipoproteins in sera from HBV-
285 infected patients. Using density gradient ultracentrifugation we detected that HBV partially
286 floated in fractions of very low density. This was corroborated by DNA dot-blot analysis and
287 HBsAg-specific ELISA indicating an association with lipoproteins of ultra-low density (**Fig**
288 **5B,C**). Interestingly, this HBV-positive, low-density fraction was not present anymore when
289 serum was filtrated through a 100 nm membrane. HBV-fractions of higher density, in contrast,
290 remained constant confirming an association with lipoproteins of very low density like
291 chylomicrons (**Fig 5D**). Furthermore, HBV started to sediment in a low-density fraction during
292 sucrose gradient ultracentrifugation when incubated with human serum (**Fig 5E**). A mixed
293 ELISA using Apo-B and Apo-E capture antibodies (**Fig 5F**) was able to detect HBV indicating
294 that HBV associates to lipoproteins. Importantly, when we subjected subviral particles to mass
295 spectrometry analysis, we detected a 28-fold enrichment of ApoE (**Fig 5G**) associated to
296 subviral particles. Finally, an association of HBV with lipoproteins was confirmed by electron

297 microscopy after immuno-gold staining (**Fig 5H**). Immuno-gold staining of HBV produced in
298 the hepatoma cell line HepAD38 that expresses endogenously ApoE detected ApoE locating
299 close to, yet distal of the virus particle which is in agreement with HBV association with an
300 ApoE-containing lipoprotein.

301

302 **ApoE enhances HBV infection and HBV localizes to cellular compartments that**
303 **accumulate free cholesterol**

304 We took advantage of a reporter virus that allows sensitive detection and quantification of HBV
305 infection by luciferase expression to address the question whether there is a functional role for
306 the HBV-lipoprotein association during infection (**Fig 6A**). Clearly, the addition of serum to HBV
307 purified by CsCl gradient centrifugation was able to enhance HBV infection of hepatocytes (left
308 panel). This effect was diminished when the serum lacked ApoE, e.g., by using the serum of
309 ApoE-deficient mice (right panel). Moreover, the infection of differentiated HepaRG-cells with
310 HBV was significantly diminished when an LDL-receptor mediated uptake was inhibited using
311 blocking antibodies during, but not after incubation of the cells with HBV (**Fig 6B**). These data
312 support the notion of an important function of HBV binding to lipoproteins for an early step of
313 HBV infection.

314 To study the intracellular transport of HBV particles and its relation to the intracellular recycling
315 pathway of lipoprotein-derived free cholesterol, we incubated liver-derived macrophages with
316 chylomicrons containing fluorescent nitrobenzoxadiazole (NBD)-cholesterol and VP₅₉₄. Two
317 hours after endocytosis of the lipoproteins - when cholesterol esters were expected to be
318 hydrolyzed - perinuclear vesicles accumulating free cholesterol also contained HBV particles
319 (**Fig 6C**). Strikingly, HBV co-incubated with human serum accumulated in Rab11-positive
320 recycling endosomes (**Figs 3,4**), which is consistent with publications reporting that free
321 cholesterol derived from ApoE-enriched TRL-remnants concentrates in recycling
322 endosomes^{20,21}. This indicates that HBV follows the recycling pathway of cholesterol derived
323 from chylomicrons in liver macrophages.

324 Recycling endosomes containing free cholesterol are intracellularly targeted by high-density
325 lipoprotein (HDL)-derived ApoA1²⁰. Since our stainings demonstrated that HBV localised in
326 liver macrophages in compartments concentrating TRL-derived free cholesterol (**Fig 6C**),
327 ApoA1-targeting provides a tool to track HBV particle transport in the macrophage. Indeed,
328 serum-derived HDL, when added to the cell culture medium, localized to vesicles containing
329 HBV particles (**Fig 6D**), and HBV, when cultured in medium containing human serum, co-
330 localised with ApoA1 (**Fig 6E**). In summary, these results demonstrate that HBV particles
331 accumulated in recycling endosomes together with lipoproteins enriched for cholesterol or
332 lipoprotein-derived cholesterol in peripheral as well as liver-derived macrophages. Our data
333 also stress the hypothesis that HBV employs the recycling pathway of lipoprotein-derived free
334 cholesterol in macrophages.

335

336 **HBV is trans-cytosed through macrophages along free cholesterol transport pathways**

337 To track the intracellular transport of HBV particles and lipoprotein-derived cholesterol in
338 macrophages, we used human monocyte-derived macrophages because they exhibit lower
339 auto-fluorescence than liver macrophages and allow more sensitive detection of specific
340 fluorescence labels. HBV particles co-localized in perinuclear and cytosolic vesicles with filipin,
341 which binds free cholesterol (**Fig 7A**). Treating macrophages with an inhibitor of cellular
342 cholesterol transport (U18666a) resulted in a perinuclear accumulation of cholesterol²². In
343 addition, transport of HBV particles from perinuclear compartments to the cell surface was
344 inhibited (**Fig 7B,C**) suggesting that HBV transport requires the free cholesterol transport
345 pathway. Thus, HBV particles not only accumulated in subcellular compartments that
346 concentrate lipoprotein-derived free cholesterol but followed the directional intracellular
347 transport and transcytosis pathways of cholesterol.

348 Release of endosomal, lipoprotein-derived free cholesterol from macrophages is induced by
349 high density lipoprotein (HDL) and HDL-derived ApoA1²⁰. Treating HBV inoculated
350 macrophages with either HDL or ApoA1 increased the secretion of HBsAg and HBV-DNA (**Fig**

351 **7D-F**). When macrophages were incubated with HBV and [³H]-cholesterol-labelled
352 chylomicrons, human serum induced their secretion and accordingly reduced their intracellular
353 concentration (**Fig 7G**). These studies confirm that HBV is secreted from macrophages in
354 analogy to cholesterol ready to enter the reverse cholesterol transport pathway to hepatocytes.

355

356 **Redistribution of HBV particles from CD68+ macrophages to hepatocytes**

357 Only hepatocytes support HBV replication and therefore are the final target cells of the virus
358 as neither macrophages nor dendritic cells support HBV replication²³. Thus, HBV particles
359 initially taken up by liver macrophages need to remain intact and be exocytosed for subsequent
360 infection of hepatocytes. To test this, human liver tissue was perfused for 45 min with VP₅₉₄
361 followed by a chase perfusion for 16h to allow for detection of redistribution of HBV particles.
362 While after 45 min HBV particles were confined to CD68+ liver macrophages (**Fig 2B-E**), after
363 the 16h chase, HBV localized within hepatocytes identified by HepPar1-staining (**Fig 8A,B**)
364 with approximately 34±9% of hepatocytes having internalized HBV. At this time point, 50±2%
365 of CD68+ liver macrophages still stained positive for HBV, but with overall fewer particles per
366 cell (**Fig 8C**).

367 Cholesterol transport directly from macrophages to hepatocytes would provide a directional
368 pathway for HBV to target hepatocytes. To investigate whether this is an option, we visualized
369 intercellular lipid transport by staining neutral lipids including cholesterol esters and free
370 cholesterol with non-polar BODIPY 493/503. Hepatocytes showed a plasma membrane
371 staining along with distinct intracellular, vesicular lipid droplets, while macrophages showed a
372 predominant intracellular staining pattern (**Fig 8D,E**). Of note, hepatocyte plasma membranes
373 in close proximity to macrophages showed a markedly enhanced lipid staining, suggesting
374 membrane lipid exchange between the cells (**Fig 8F**). Additionally, macrophage membrane
375 protein CD68 was detected in hepatocyte cell membranes closely located to liver
376 macrophages, supporting the hypothesis of a direct intercellular membrane component
377 exchanges (**Fig 8G**). In hepatocytes, HBV was exclusively detected at plasma membranes

378 with enhanced lipid staining (**Fig 8D**), or within lipid containing structures proceeding from the
379 plasma membrane into the interior of the hepatocyte (**Fig 8E**) supporting our model of reverse
380 transport of HBV from macrophages to hepatocytes.

381

382 **HBV particles taken up by liver macrophages trans-infect hepatocytes**

383 To characterize whether liver macrophages promote HBV-infection of hepatocytes in trans, we
384 set up co-cultures of primary human liver macrophages and hepatocytes isolated from the
385 same donor. Liver macrophages were loaded with VP₅₉₄ and any unbound virus removed by
386 intensive washing before co-culturing with chloromethylfluorescein diacetate (CMFDA)
387 labelled hepatocytes. After an overnight co-culture, HBV was detected within CMTDA+
388 hepatocytes (**Fig 9A**). Of note, we observed filamentous intercellular connections (**Fig 9B**,
389 **arrow**), and an exchange of Dil-labeled membrane patches between macrophages and
390 hepatocytes (**Fig 9C**).

391 To evaluate whether macrophages can transfer infectious HBV to hepatocytes, liver
392 macrophages were incubated with HBV at either 4°C or 37°C for 6h, washed, trypsinized and
393 incubated with primary human hepatocytes at 37°C for 12 days (**Fig 9D**). Only incubation at
394 37°C that allowed virus uptake into macrophages resulted in HBV infection of hepatocytes,
395 establishment of cccDNA (**Fig 9E**) and secretion of HBeAg and HBsAg (**Fig 9F**) while
396 macrophage incubation at 4°C that did not allow for virus uptake did not result in HBV infection
397 of hepatocytes (**Fig 9E,F**). Importantly, liver macrophages themselves were not productively
398 infected (**Fig 9G**). Trans-infection was blocked by the entry-inhibitor Bulevirtide and
399 neutralizing anti-HBs antibodies (**Fig 9H**) illustrating that trans-infection is also dependent on
400 the bona fide HBV receptor. In addition, trans-infection was significantly reduced upon
401 U18666-mediated inhibition of cholesterol efflux from macrophages (**Fig 9I**). However, trans-
402 infection of hepatocytes with HBV via liver macrophages was not more efficient than direct
403 infection of hepatocytes, suggesting trans-infection via liver macrophages is not necessarily a
404 preferential but rather an alternative infection route, at least *in vitro* (**Fig 9J**). Taken together,

405 our findings show that macrophages can internalize HBV, form intercellular membrane bridges
406 that could potentially promote cell-to-cell transmission of HBV and trans-infect hepatocytes via
407 a cholesterol efflux-dependent pathway.

408 **Discussion**

409 HBV infection relies on very efficient targeting of permissive hepatocytes since one single virus
410 is able to establish infection in a chimpanzee¹. It remained unclear how HBV is able to reach
411 the liver without being phagocytosed in the circulation, how it bypasses liver scavenger cells
412 and how it is able to selectively target hepatocytes for infection. Here, we characterize these
413 early steps of HBV uptake into the liver under physiological conditions using a novel liver
414 perfusion and infection model that allowed us to track HBV in liver tissue. Interestingly, HBV
415 was rapidly taken up into liver macrophages and only at a later time point detected in
416 hepatocytes. We found that HBV associates with human serum lipoproteins and ApoE. Within
417 macrophages, HBV localized to the same endosomal compartments as lipoproteins before
418 being released along the cholesterol efflux pathway. HBV released after trans-infection of
419 macrophages was able to infect hepatocytes. Since lipoprotein and reverse cholesterol
420 transport to the liver is an efficient physiological process, we hypothesise that HBV exploits
421 this pathway to reach the liver and infect hepatocytes.

422 Accordingly, we propose the following model for HBV host cell targeting. HBV - after
423 association with ApoE-rich lipoproteins - attaches to liver-specific HSPG that protrude from the
424 Space of Disse across endothelial fenestration into the liver sinus²⁴. Subsequently, HBV may
425 be taken up directly into hepatocytes or first into liver macrophages. The ratio of direct host
426 cell targeting vs. trans-infection is likely to be determined by individual lipidemic¹⁷ and/or
427 microstructural liver sinus²⁵ conditions. HBV sequestered by liver macrophages, hijacks the
428 intracellular lipoprotein metabolism and is re-secreted along the free cholesterol-recycling
429 pathway. Free cholesterol and HBV are then delivered from the macrophages via intercellular
430 membrane bridges to neighbouring hepatocyte plasma membranes where interaction with the
431 HBV receptor NTCP can prime a productive infection. Thus, the hepatotropism of HBV as well
432 its ability to survive within the circulation may depend on the utilization of cellular lipid transport
433 pathways that are hepatocyte-directed.

434 The bile-acid transporter peptide NTCP has recently been identified as a HBV receptor that is
435 exclusively expressed on hepatocytes². How HBV gains access to hepatocellular NTCP *in vivo*
436 is not understood since endothelial cells lining the sinusoids restrict passive diffusion of
437 particles >12 nm in diameter²⁵. Since HBV is an enveloped virus with a diameter of 42 nm, it
438 seems unlikely that HBV can passively diffuse through this layer of sinusoidal cells with the
439 efficiency needed to promote the high *in vivo* particle infectivity that has been reported¹.
440 Moreover, one has to consider the scavenging activity of LSECs and liver macrophages that
441 could easily trap and lyse HBV. A directed transport exploiting a transcytosis pathway through
442 macrophages as we have observed would be able to overcome these hurdles. Preferential
443 uptake of HBV by liver macrophages - as we observed *in vivo* in mice - may result from initial
444 binding to liver specific HSPG^{3,4} extending into the liver sinus. Binding to these HSPG has
445 been observed e.g. for plasmodium sporozoites²⁴.

446 Since HBV does not require distinct glycosaminoglycans found in the liver to confer hepatocyte
447 specificity³, the association with serum components like lipoprotein remnants may increase
448 targeting to hepatic glycosaminoglycans and other lipoprotein receptors. This reasoning is
449 supported by our and others recent findings that liver uptake is significantly reduced in ApoE-
450 deficient mice and that HBV infection is inhibited by ApoE-specific antibodies *in vitro*,
451 respectively^{13,14}, as well as by reports that HBV binds to ApoH and lipoprotein lipase^{26,27}, both
452 surface components of lipoproteins. In our study we demonstrate that HBV associates with
453 lipoproteins in patients' serum and when release from producer cells, and that blocking LDL-
454 receptor function on hepatocytes markedly reduces productive infection. Importantly, efficient
455 hepatocyte infection relied on the presence of ApoE supporting the crucial role of an
456 association of HBV to ApoE-containing lipoproteins.

457 Electron microscopy analysis after immunogold staining strongly supported the association of
458 HBV with ApoE-containing lipoproteins. Interestingly, ApoE was detected distal of the virus
459 particle in accordance with an association of a lipid particle smaller than 100 nm in diameter,
460 presumably an ApoE-containing HDL or a small VLDL/LDL. An exact quantification of the HBV-

461 lipoprotein association, however, is difficult since the purification of HBV requires
462 ultracentrifugation that is known to dissociate proteins from lipoproteins²⁸. As the virus-
463 lipoprotein association rather is of lower affinity, virions may have dissociated during
464 purification resulting in an underestimation of the association of HBV with lipoproteins of low
465 density in our experiments.

466 In addition to mediating liver-tropism, lipoprotein embedded cholesterol may facilitate HBV
467 recycling within macrophages as described for lipoprotein-associated proteins like ApoC, ApoE
468 and lipoprotein lipase²¹. Lipoproteins bind to LDL-receptors on hepatocytes via ApoE, that has
469 allelic variants ApoE1 to 4. ApoE3 more potently binds the LDL-receptor and induces cellular
470 cholesterol recycling than its allelic variants²⁹. Interestingly, the ApoE3 allele is
471 overrepresented in HBV-infected patients and subjects with an ApoE3 allele have a lower rate
472 of spontaneous HBsAg clearance^{30,31}. Thus, clinical observations support an important role of
473 lipoprotein metabolism and transport to the liver in early HBV infection. Finally, association of
474 HBV infection with lipoprotein-metabolism is further supported by inhibition of an early infection
475 step by lipase inhibitor Orlistat¹³.

476 The contribution of macrophages to reverse cholesterol transport represents a physiological
477 pathway, by which cholesterol derived from circulating lipoproteins is endocytosed into
478 recycling endosomes in macrophages, effluxed to lipid acceptors and delivered to hepatocytes,
479 especially under hyperlipidemic conditions and in the postprandial situation^{15,17}. Lipids effluxed
480 from liver macrophages are incorporated into hepatocytes *in vivo*¹⁷. The N-terminal acyl
481 residue of the HBV L protein may mediate transport along the free cholesterol transport
482 pathway as described for influenza hemagglutinin³² and other acylated proteins including
483 glycosylphosphatidylinositol anchored proteins.

484 Liver resident macrophages are located in close proximity to hepatocytes that are specialised
485 in cholesterol uptake. Intercellular membrane bridges between neighbouring donor and
486 acceptor cells have been suggested to support lipid transport³³. We observed intercellular
487 membrane bridges between liver resident macrophages or Kupffer cells and hepatocytes and

488 the transfer of lipids and membrane proteins from Kupffer cell to hepatocyte membranes
489 suggest a direct exchange of membrane components between neighbouring cells. This
490 principle is exploited by prions, which - as HBV - recycle along the free cholesterol pathway to
491 the plasma membrane and are directly transferred to neighbouring cells via membrane
492 bridges^{34,35}. Thus, routing along the recycling cholesterol transport pathway in liver
493 macrophages and transcellular delivery to hepatocytes through intercellular membrane bridges
494 appear to act in concert to facilitate hepatocyte-targeting by HBV.

495 In conclusion, it seems that as for other viruses, specific host cell targeting by HBV does not
496 only result from a particular virus-receptor interaction on the target cell. Our results propose
497 that HBV *in vivo* associates with lipoproteins, may take advantage of their liver targeting and
498 is able to hijack the cholesterol transport pathway through macrophages. These pathways
499 have been evolutionary optimized to deliver their cargo from distant sites to the liver and may
500 explain the highly efficient liver targeting by HBV. They are suited to support the deposition of
501 HBV in the perisinusoidal Space of Disse from where HBV can bind its receptor on hepatocytes
502 or even be directly transport to hepatocytes by the establishment of membrane bridges.

503

504 **Materials and Methods**

505 All authors had access to the study data and had reviewed and approved the final manuscript.

506 For additional details on materials, providers and procedures see Supplemental Information.

507

508 ***Ex vivo* human liver perfusion**

509 HBV viral particles were purified by sequential sucrose and CsCl gradient sedimentations and
510 fluorescence labelled with Alexa Fluor 594® (VP₅₉₄). Human liver tissue samples and
511 annotated data were obtained and experimental procedures were performed within the
512 framework of the non-profit foundation HTCR, including the informed patient's consent.
513 Surgical human liver biopsies (10 to 20 g) consisting of healthy tissue obtained during
514 metastasis resection were perfused within 2 hours with medium containing HBV, VP₅₉₄ and

515 human serum as indicated via portal vein branches at 37°C. To potentially increase HBV-TRL-
516 associations, postprandial but not preprandial serum was used. For longer perfusions, 12%
517 erythrocytes were added and oxygen was supplied.

518 **Virus uptake into liver cells**

519 Primary human hepatocytes and liver macrophages were isolated by two-step collagenase
520 perfusion followed by differential centrifugation and adherence steps and maintained as
521 described³⁶. Human serum negative for anti-HBs antibodies and monocytes for differentiation
522 into macrophages were obtained from healthy volunteers.

523 Liver macrophages were incubated with HBV at a multiplicity of infection (MOI) of 100
524 enveloped, DNA-containing HBV particles, washed five times, trypsinized at 37°C for 15
525 minutes, centrifugated for 5 min at 300 g, adhered to the culture surface for 1h, three times
526 washed and subsequently hepatocytes were seeded on top. Re-secretion and (trans-)infection
527 were monitored by determining HBsAg, HBeAg and HBV-DNA in cell culture supernatant. HBV
528 cccDNA was determined in infected hepatocyte lysates by quantitative RT-PCR²³. HBV RNA
529 was isolated using the Monarch Total RNA Miniprep Kit according to the manufacturer's
530 protocol but with 1h of DNase digestion. cDNA was synthesized with LunaScript RT SuperMix
531 Kit (with a denaturation step of the RNA for 5 min 95°C, incubation on ice, 50 min 50°C, 5 min
532 95°C) (both New England Biolabs, Ipswich, MA, USA). For qPCR, primers/probes from Life
533 Technologies (Thermo Fisher, Frankfurt, Germany) were used.

534 To analyse the functional contribution of lipoproteins, recombinant (r)HBV expressing
535 NanoLuc-Luciferase (rHBV-Luc) was produced as previously described³⁷ that allows for a
536 sensitive and quantitative infection. To remove supernatant- and particle-associated proteins,
537 recombinant rHBV-Luc was highly purified via heparin-affinity chromatography and
538 subsequent sucrose- and CsCl-gradient ultracentrifugation. rHBV-Luc particles were
539 concentrated and buffer exchanged in PBS, and cells were infected with the highly purified
540 rHBV in the presence or absence of 10% FCS, or serum obtained from CH57B6/N wild-type
541 or ApoE-knockout mice. To determine infection efficacy, 10 µL cell culture supernatant were

542 mixed with 100 μ L PBS containing 0.1% Tween 20 and 1 μ M Coelenterazine N as described³⁸.
543 Luminescence was detected using a Tecan Infinite 200 reader (Tecan Group Männedorf,
544 Switzerland).

545 **Isolation of mouse hepatocytes and liver macrophages**

546 Mouse livers were perfused by a standard two-step collagenase perfusion through the portal
547 vein *in situ* before the liver was collected and the tissue was homogenized and passed through
548 a cell strainer. The cell suspension was incubated with magnetic CD11b-specific MicroBeads
549 and loaded onto a MACS column (both Miltenyi Biotec, Bergisch Gladbach, Germany) to
550 collect macrophages according to the manufactures protocol. The remaining cell solution was
551 centrifuged twice for 5 minutes at 50 g without break to collect hepatocytes.

552 **Re-secretion from macrophages**

553 THP macrophages were differentiated with 70 nM phorbol-12-myristate-13-acetate and
554 incubated with 1×10^8 HBV virions / ml (final concentration) for 3 hours and subsequently
555 without HBV, but adding 10% human serum, 100 or 200 μ g/ml HDL as indicated. To determine
556 cholesterol secretion, 1 μ g/ml [3H]-cholesterol-chylomicrons were added to the HBV
557 incubation, and heparin was added to the washing. [3H]-cholesterol was quantified in
558 supernatant and cell lysates by liquid scintillation counting.

559 **Electron microscopy of liver tissue**

560 10 μ m cryosections of liver tissue or PFA-fixed cells were permeabilized with PBS / 0.5%
561 saponin and stained with appropriate primary and indicated secondary antibodies. To stain
562 neutral lipids BODIPY493/503 (1/250), to stain free cholesterol 50 μ g/ml filipin was used. All
563 images were acquired on an Olympus FluoView 1000-confocal laser-scanning microscope.
564 For transmission electron microscopy, liver tissue was fixed with 2.5% glutaraldehyde in 0.1
565 mol/l cacodylate, post-fixed with 1% OsO₄ and stained with uranyl acetate followed by lead
566 citrate. Ultra-thin section were analyzed on a Zeiss EM 10 CR electron microscope (Zeiss,
567 Oberkochen, Germany).

568 **Immuno-gold staining and electron microscopy of HBV virions**

569 Sucrose fractions containing HepAD38 cell-derived HBV virions were diluted with TN buffer
570 (20 mM Tris-HCL pH 7.4 and 140 mM NaCl) and fixed with 2% PFA for 4 hours at 40°C.
571 Residual sucrose and PFA were removed by using Amicon Ultra (30k) centrifugal filter units
572 by diluting and washing concentrated samples with TN buffer. Freshly glow-discharged
573 carbon- and pioloform-coated 300-mesh copper grids (Science Services GmbH, Munich,
574 Germany) were floated on top of 10 µl of different dilutions of sucrose-free HBV particles for 5
575 minutes. After removal of the sample by soaking into Whatman paper, the grid was briefly
576 washed by floating on a droplet of 3% uranylacetate (UA) solution, followed by another floating
577 on a fresh 3% UA droplet for 2 minutes. The stain was removed by soaking into Whatman
578 paper and the grid was air-dried at room temperature before staining and imaging with a JEOL
579 JEM-1400 transmission electron microscope (Jeol GmbH, Freising, Germany).

580 Quality of the HBV virion-containing samples was assessed by TEM analysis of negatively
581 stained samples. Immuno-gold labeling that was performed as described elsewhere³⁹. In brief,
582 samples absorbed onto glow-discharged grids were washed with H₂O, incubated for 20
583 minutes in blocking buffer (0.8% BSA, 0.1% fish skin gelatin, 50 mM glycine in PBS) and
584 incubated with primary antibodies for 20 minutes in blocking buffer, followed by 5-times
585 washing of the grids with PBS before incubation of the grids with Protein A-10 nm gold
586 conjugate (Cell Microscopy Core, NL) in blocking solution for 20 minutes. The antibodies used
587 for immuno-gold labeling were anti-ApoE (Sigma-Aldrich - AB947), anti-HBsAg (Humabs
588 Biomed – HBC34) and goat-IgG isotype control (Santa Cruz – Sc2028). Thereafter, the grids
589 were washed again with PBS and fixed with 1% glutaraldehyde in PBS for 5 minutes.

590 **Mass spectrometry of purified HBV subviral particle fractions**

591 Subviral particles were produced in HepG2 cells stably transfected with a plasmid encoding
592 HBV genome 2415-1839 expressing all three HBV surface proteins (HepG2-LMS). Particles
593 were purified as previously described via heparin-affinity chromatography and sucrose
594 gradient ultracentrifugation⁴³. Fractions containing the subviral particles were collected,

595 concentrated and buffer exchanged to PBS using VivaSpin 6 filter units (100 000 MWCO,
596 Sartorius) and analyzed via liquid chromatography/mass spectrometry (LC/MS) using an
597 Orbitrap Eclipse Tribrid mass spectrometer (Thermo Fisher). Supernatant of HepG2 cells not
598 expressing HBV proteins was purified as control. A HepG2-LMS and HepG2 control sample
599 were denatured with urea lysis buffer (8 M Urea, 50 mM Tris-HCl pH 7.5) followed by reduction
600 with 10 mM DTT for 45 min at 30°C and alkylation of cysteines with 55 mM CAA for 30 min at
601 room temperature. Samples were diluted 1:5 with digestion buffer (Tris-HCl pH 8.5, 2 mM
602 CaCl₂) and digested with trypsin at 1:50 enzyme-to-protein ratio at 37°C overnight. Samples
603 were acidified with 1% formic acid (FA) followed by desalting on self-packed StageTips.
604 Peptides were eluted with 50% ACN, 0.1 % FA and dried down prior to LC-MS/MS analysis.
605 LC-MS/MS measurements were performed on a Dionex Ultimate 3000 RSLCnano system
606 coupled to an Orbitrap Eclipse mass spectrometer (ThermoFisher Scientific, Bremen). Peptides
607 were reconstituted in 0.1% FA and measured in data dependent acquisition mode with a 50
608 min linear LC gradient. Peptide and protein identification and quantification was performed with
609 MaxQuant software (v. 1.6.3.3) with standard settings unless otherwise described⁴⁴. Raw files
610 were searched against the human and bovine reference proteome (UP000005640, download
611 01/2021; UP000009136, download 04/2022), a customized HBV sequence fasta file and
612 common contaminants. Carbamidomethylated cysteine was set as fixed modification and
613 oxidation of methionine, and N-terminal protein acetylation as variable modifications. Trypsin/P
614 was specified as the proteolytic enzyme with up to two missed cleavage sites allowed. Results
615 were adjusted to 1% peptide spectrum match and 1% protein false discovery rate (FDR).
616 Displayed protein abundances are based on log₂ transformed median centered iBAQ
617 intensities.

618 **Statistical analysis**

619 Data are given as mean \pm SD unless otherwise indicated. Statistical analysis was performed
620 using unpaired student's t-test or by Two-Way ANOVA when more than two groups were
621 compared.

622 **Confirmatory statement**

623 All authors had access to the study data. Additionally, the final manuscript has been reviewed
624 and approved by all authors.

625

626 **Acknowledgements**

627 The authors thank Luise Jennen, Lilianna Schyschka and Raindy Tedjokusumo for excellent
628 technical support, Jörg Kleeff and Sonja Gillen for support with the ethic's application and
629 patient information, and Jane McKeating for critically reading the manuscript. We are grateful
630 to the Heidelberg University electron microscopy core facility, headed by Charlotta Funaya.
631 We acknowledge the support of the non-profit foundation HTCR, which holds human tissue on
632 trust, making it broadly available for research on an ethical and legal basis.

633

634 **References**

- 635 1. Asabe, S. *et al.* The Size of the Viral Inoculum Contributes to the Outcome of Hepatitis B Virus
636 Infection. *J. Virol.* (2009). doi:10.1128/jvi.00867-09
- 637 2. Yan, H. *et al.* Sodium taurocholate cotransporting polypeptide is a functional receptor for
638 human hepatitis B and D virus. *Elife* **2012**, (2012).
- 639 3. Leistner, C. M., Gruen-Bernhard, S. & Glebe, D. Role of glycosaminoglycans for binding and
640 infection of hepatitis B virus. *Cell. Microbiol.* **10**, 122–133 (2008).
- 641 4. Schulze, A., Gripon, P. & Urban, S. Hepatitis B virus infection initiates with a large surface
642 protein-dependent binding to heparan sulfate proteoglycans. *Hepatology* **46**, 1759–1768
643 (2007).
- 644 5. Protzer, U., Maini, M. K. & Knolle, P. A. Living in the liver: Hepatic infections. *Nature Reviews*
645 *Immunology* (2012). doi:10.1038/nri3169
- 646 6. Gardner, J. P. *et al.* L-SIGN (CD 209L) is a liver-specific capture receptor for hepatitis C virus.
647 *Proc. Natl. Acad. Sci. U. S. A.* (2003). doi:10.1073/pnas.0831128100
- 648 7. Lai, W. K. *et al.* Expression of DC-SIGN and DC-SIGNR on human sinusoidal endothelium: A
649 role for capturing hepatitis C virus particles. *Am. J. Pathol.* (2006).

- 650 doi:10.2353/ajpath.2006.051191
- 651 8. Cormier, E. G. *et al.* L-SIGN (CD209L) and DC-SIGN (CD209) mediate transinfection of liver
652 cells by hepatitis C virus. *Proc. Natl. Acad. Sci. U. S. A.* (2004). doi:10.1073/pnas.0405695101
- 653 9. Rowe, I. A. *et al.* Paracrine signals from liver sinusoidal endothelium regulate hepatitis C virus
654 replication. *Hepatology* (2014). doi:10.1002/hep.26571
- 655 10. Breiner, K. M., Schaller, H. & Knolle, P. A. Endothelial cell-mediated uptake of a hepatitis B
656 virus: A new concept of liver targeting of hepatotropic microorganisms. *Hepatology* (2001).
657 doi:10.1053/jhep.2001.27810
- 658 11. Frevert, U. *et al.* Intravital observation of plasmodium berghei sporozoite infection of the liver.
659 *PLoS Biol.* (2005). doi:10.1371/journal.pbio.0030192
- 660 12. Tavares, J. *et al.* Role of host cell traversal by the malaria sporozoite during liver infection. *J.*
661 *Exp. Med.* (2013). doi:10.1084/jem.20121130
- 662 13. Esser, K. *et al.* Lipase inhibitor orlistat prevents hepatitis B virus infection by targeting an early
663 step in the virus life cycle. *Antiviral Res.* (2018). doi:10.1016/j.antiviral.2018.01.001
- 664 14. Qiao, L. & Luo, G. G. Human apolipoprotein E promotes hepatitis B virus infection and
665 production. *PLoS Pathog.* (2019). doi:10.1371/journal.ppat.1007874
- 666 15. Ikonen, E. Cellular cholesterol trafficking and compartmentalization. *Nat. Rev. Mol. Cell Biol.* **9**,
667 125–138 (2008).
- 668 16. Richard, B. M. & Pittman, R. C. ROLE OF HDL1 IN CHOLESTERYL ESTER UPTAKE IN
669 RATS. *J. Lipid Res.* **34**, 571–579 (1993).
- 670 17. van DIJK, M. C. M., ZIERE, G. J. & van BERKEL, T. J. C. Characterization of the chylomicron-
671 remnant-recognition sites on parenchymal and Kupffer cells of rat liver Selective inhibition of
672 parenchymal cell recognition by lactoferrin. *Eur. J. Biochem.* (1992). doi:10.1111/j.1432-
673 1033.1992.tb16842.x
- 674 18. Mahley, R. W. & Ji, Z. S. Remnant lipoprotein metabolism: Key pathways involving cell-surface
675 heparan sulfate proteoglycans and apolipoprotein E. *Journal of Lipid Research* (1999).
- 676 19. Roingeard, P. & Sureau, C. Ultrastructural analysis of hepatitis B virus in HepG2-transfected
677 cells with special emphasis on subviral filament morphogenesis. *Hepatology* (1998).
678 doi:10.1002/hep.510280431
- 679 20. Heeren, J. *et al.* Recycling of apoprotein E is associated with cholesterol efflux and high
680 density lipoprotein internalization. *J. Biol. Chem.* (2003). doi:10.1074/jbc.M209006200
- 681 21. Heeren, J., Grewal, T., Jäckle, S. & Beisiegel, U. Recycling of Apolipoprotein E and Lipoprotein
682 Lipase through Endosomal Compartments in Vivo. *J. Biol. Chem.* (2001).
683 doi:10.1074/jbc.M107461200

- 684 22. Higgins, M. E., Davies, J. P., Chen, F. W. & Ioannou, Y. A. Niemann-pick C1 is a late
685 endosome-resident protein that transiently associates with lysosomes and the trans-Golgi
686 network. *Mol. Genet. Metab.* (1999). doi:10.1006/mgme.1999.2882
- 687 23. Untergasser, A. *et al.* Dendritic cells take up viral antigens but do not support the early steps of
688 hepatitis B virus infection. *Hepatology* **43**, 539–547 (2006).
- 689 24. Pradel, G., Garapaty, S. & Frevert, U. Proteoglycans mediate malaria sporozoite targeting to
690 the liver. *Mol. Microbiol.* (2002). doi:10.1046/j.1365-2958.2002.03057.x
- 691 25. Kempka, G. & Kolb-Bachofen, V. Binding, uptake, and transcytosis of ligands for mannose-
692 specific receptors in rat liver: An electron microscopic study. *Exp. Cell Res.* (1988).
693 doi:10.1016/0014-4827(88)90118-8
- 694 26. Stefas, I. *et al.* Hepatitis B virus Dane particles bind to human plasma apolipoprotein H.
695 *Hepatology* (2001). doi:10.1053/jhep.2001.20531
- 696 27. Deng, Q. *et al.* Identification and characterization of peptides that interact with hepatitis B virus
697 via the putative receptor binding site. *J. Virol.* **81**, 4244–54 (2007).
- 698 28. Heeren, J., Niemeier, A., Merkel, M. & Beisiegel, U. Endothelial-derived lipoprotein lipase is
699 bound to postprandial triglyceride-rich lipoproteins and mediates their hepatic clearance in vivo.
700 *J. Mol. Med.* (2002). doi:10.1007/s00109-002-0351-5
- 701 29. Schneider, W. J., Kovanen, P. T. & Brown, M. S. Familial dysbetalipoproteinemia. Abnormal
702 binding of mutant apoprotein E to low density lipoprotein receptors of human fibroblasts and
703 membranes from liver and adrenal of rats, rabbits, and cows. *Journal of Clinical Investigation*
704 **68**, 1075–1085 (1981).
- 705 30. Toniutto, P. *et al.* Genetic polymorphism at the apolipoprotein E locus affects the outcome of
706 chronic hepatitis B. *J. Med. Virol.* **82**, 224–231 (2010).
- 707 31. Ahn, S. J. *et al.* Association between apolipoprotein E genotype, chronic liver disease, and
708 hepatitis B virus. *Clin. Mol. Hepatol.* **18**, 295–301 (2012).
- 709 32. Melkonian, K. A., Ostermeyer, A. G., Chen, J. Z., Roth, M. G. & Brown, D. A. Role of lipid
710 modifications in targeting proteins to detergent-resistant membrane rafts. Many raft proteins
711 are acylated, while few are prenylated. *J. Biol. Chem.* (1999). doi:10.1074/jbc.274.6.3910
- 712 33. Rustom, A., Saffrich, R., Markovic, I., Walther, P. & Gerdes, H. H. Nanotubular Highways for
713 Intercellular Organelle Transport. *Science* (80-.). (2004). doi:10.1126/science.1093133
- 714 34. Gilch, S., Bach, C., Lutzny, G., Vorberg, I. & Schätzl, H. M. Inhibition of cholesterol recycling
715 impairs cellular PrPSc propagation. *Cell. Mol. Life Sci.* (2009). doi:10.1007/s00018-009-0158-4
- 716 35. Gousset, K. *et al.* Prions hijack tunnelling nanotubes for intercellular spread. *Nat. Cell Biol.*
717 (2009). doi:10.1038/ncb1841

- 718 36. Ebert, G. *et al.* 5' triphosphorylated small interfering RNAs control replication of hepatitis B
719 virus and induce an interferon response in human liver cells and mice. *Gastroenterology* **141**,
720 (2011).
- 721 37. Wing, P. A. C. *et al.* Hypoxia inducible factors regulate hepatitis B virus replication by activating
722 the basal core promoter. *J. Hepatol.* **75**, 64–73 (2021).
- 723 38. Ryu, J. *et al.* Rapid, accurate mapping of transgene integration in viable rhesus macaque
724 embryos using enhanced-specificity tagmentation-assisted PCR. *Mol. Ther. Methods Clin.*
725 *Dev.* **24**, 241–254 (2022).
- 726 39. Pham, M. *et al.* Endosomal egress and intercellular transmission of hepatic ApoE-containing
727 lipoproteins and its exploitation by the hepatitis C virus. Preprint from bioRxiv (2022).
- 728 40. Wettengel, J. M. *et al.* Rapid and Robust Continuous Purification of High-Titer Hepatitis B Virus
729 for In Vitro and In Vivo Applications. *Viruses* **13**, (2021).
- 730

731 Figure Legends

732

733 Fig 1: Establishment of an *ex vivo* perfusion model of human liver tissue.

734 (A) Schematic depiction of the *ex vivo* perfusion system. Inside a cell culture incubator, liver
735 tissue was kept in a sterile container filled with medium containing human serum. Using a
736 perfusion pump, the tissue piece was continuously perfused via branches of the portal vein.
737 (B) Liver tissue was perfused for 17 h with 50% human serum containing medium. For 30 min,
738 20 µg/ml Alexa Fluor®647-labelled ovalbumin was added to assess receptor mediated
739 endocytosis and confirm intact liver cell function. Fixed liver tissue sections were analysed by
740 confocal laser scanning microscopy. (C) Purified HBV particles were subjected to 10% SDS-
741 PAGE before (left) or after Alexa594 fluorochrome-labeling (VP₅₉₄, right). Gels were either
742 silver stained (left) or investigated for fluorescence ($\lambda_{ex}/\lambda_{em}$ = 365/602, right). Arrows
743 indicate large (L), middle (M) and small (S) envelop proteins at expected molecular weight
744 (kDa). (D) Isolated liver macrophages were incubated with medium containing VP₅₉₄ for 1h
745 before cells were washed and fixed. Cells were stained with HBsAg-specific antibodies and
746 Alexa488-labelled secondary antibodies. Merged pictures show VP₅₉₄ in red and HBsAg in
747 green with arrows pointing at co-localising VP₅₉₄ with HBsAg-specific staining. (E) After 45 min
748 perfusion with unlabelled HBV VP liver tissue sections were stained with polyclonal rabbit anti-
749 HBs and fluorescent secondary antibodies (left panel). As control, perfused tissue was stained
750 with rabbit control serum (right panel) to confirm specificity of HBsAg-detection. (F) Liver tissue
751 of an HCV-infected, but HBV-negative patient was fixed and stained with HBsAg- and CD68-
752 specific primary and fluorescent secondary antibodies showing no HBsAg-detection in HBV-
753 negative tissue. Scale bar is 10 µm in (B, D-F).

754

755 Fig 2: Uptake of HBV particles by liver macrophages in *in vivo* perfused human livers.

756 (A) Human liver tissue pieces were perfused at 37°C with medium containing 5x10⁹ HBV
757 virions/ml and 50% human serum for 17h and subsequently with medium only for 58h. Before
758 and at the end of perfusion, tissue sections were lysed and DNA was extracted. HBV cccDNA
759 content was determined by a selective real time PCR and is given relative to cellular PRNP
760 gene expression, each dot represents a randomly taken liver tissue sample (left panel);
761 perfusate was analysed for HBeAg content by ELISA (mean ± SD of OD₄₅₀, duplicates), a
762 separate piece of liver tissue from the same donor perfused with HBV-negative medium served
763 as negative control (right panel). (B-F) Human liver tissue pieces were perfused at 37°C for 45
764 min with medium containing 50% human serum and 10¹⁰ VP₅₉₄/ml (shown in red), and fixed
765 tissue sections were stained for macrophage marker CD68 (shown in green). (B) Differential
766 interference contrast (DIC) showing liver sinusoids with hepatocytes next to CD68-stained liver
767 macrophages. (C) Quantification of CD68⁺ or CD68⁻, HBV+ cells. Analysis of ten random vision
768 fields (200-fold magnification; mean values ± SD). (D) XY- and Z-axis projection at higher
769 magnification to visualize intracellular localization of VP₅₉₄ in macrophages (y-z), cell nucleus
770 stained with DAPI. (E) Immunofluorescence staining for CD68 and HBsAg in fixed tissue
771 sections perfused with non-labelled HBV. (F) Immunostaining of liver tissue from a chronically
772 infected HBV patient for HBsAg (shown in red) and CD68 (shown in green). Lower row shows
773 the boxed area enlarged. (G-I) CH57Bl/6 mice were intravenously injected through the tail vein
774 with (G,H) 2x10¹¹ FITC (VP_{FITC}) labelled VP or (I) 1x10⁹ virions purified from HBV-positive
775 plasma after filtration through a 100 nm pore size filter. (G) After 45 min mouse livers were
776 fixed, liver sections were stained with macrophage maker F4/80 and analysed by confocal

777 laser-scanning microscopy. Y-axis (y-z) and z-axis projections (x-z) are shown. Merged
778 pictures show VP_{FITC} in green. (H) Numbers of VP_{FITC}-positive, F4/80+/- cells (ten randomly
779 selected vision fields at 200-fold magnification). (I) 1h after injection, liver macrophages and
780 hepatocytes were isolated. Cellular DNA was prepared and analysed by quantitative RT-PCR
781 for HBV-DNA relative to NID2 as house-keeping gene. Values are mean ± SEM of two
782 independent experiments, with triplicates analyzed per experiment. **p=0,0012. All scale bars
783 are 10 µm.

784

785 **Fig 3: HBV cellular localisation in human primary liver macrophages.**

786 (A) Primary human liver macrophages were incubated with purified HBV for 4 h either at 37°C
787 or 4°C, and after washing were lysed and HBV DNA was quantified by qPCR. Means±SD of
788 one representative experiment with three independent replicates in each group are shown.
789 *p<0.5. (B-E) Liver macrophages were incubated with VP₅₉₄ in medium containing 10% human
790 serum for 1h, thoroughly washed and either immediately fixed (B,C) or further cultivated for
791 16h in absence of HBV to follow intracellular transport of HBV (D, E). After fixation cells were
792 stained for LAMP1 (B and D) or Rab11 (C and E). Merged pictures show VP₅₉₄ in red, CD 68,
793 LAMP1, and Rab11 staining in green, and nuclear staining with DAPI in blue. Representative
794 images of single liver macrophages are shown, scale bars are 10 µm.

795

796 **Fig 4: Differential localization of HBV and recombinant HBsAg in THP macrophages.**

797 THP macrophages were incubated with medium containing fluorochrome-labelled HBV (VP₅₉₄;
798 A, B, D, F) or recombinant HBsAg (HBsAg₅₉₄; C, E, G) for 1h. Cells were either directly fixed
799 after washing (A) or further cultivated without HBV for 16h (B, C) and stained for Rab11. (D-
800 G) Cells were either directly fixed after washing (D, E) or after further cultivation without HBV
801 or HBsAg for 16 h (F, G) and stained for LAMP1. Merged pictures show VP₅₉₄ and HBsAg₅₉₄
802 in red, Rab11 and LAMP1 in green, and nuclear staining with DAPI in blue. Scale bar 10 µm.
803 Co-localization determined in three randomly selected vision fields of each group was analyzed
804 using Manders' correlation method. Mred (fraction of red overlapping with green) was
805 calculated using JACoP plugin of ImageJ. The means±SD of four random views of one
806 representative experiment are shown as bar graphs next to the respective image. ***p<0.001,
807 ****p<0.0001.

808

809 **Fig 5: Association of HBV with lipoproteins.** (A) Human liver tissue was perfused for 45
810 min at 37°C with medium containing human serum and HBV (perfused tissue) or directly fixed
811 without perfusion with HBV (non-perfused tissue) as negative control. Transmission electron
812 microscopy shows liver macrophages (KC) next to a hepatocyte (Hep) in HBV perfused and
813 non-perfused liver tissue (left panels), areas marked in red are shown at higher magnification
814 (right panels). Exemplary sections are shown, demonstrating co-localization of triglyceride-rich
815 lipoprotein (TRL) and HBV particles in perfused livers (white arrows) and an example of
816 lipoproteins in a non-perfused liver (dark arrows). Scale bars indicate 1µm (left panels) and
817 100nm (right panels) LD: lipid droplets; Ery: erythrocytes. (B-D) The plasma sample of an HBV
818 infected patient was separated by sucrose density gradient ultracentrifugation either directly
819 (B,C) or after filtration through a membrane of 100 nm pore size (D). Indicated fractions (Fr.)
820 were analysed for HBV-DNA by dot blot-analysis (B,D) and for HBsAg content by ELISA (C).
821 (B,D) Volumes dotted are indicated above, HBV-DNA-content and density of each fraction are
822 given below the dot blots. (C) HBsAg content of ultra-low density fractions 25 and 26 from non-

823 filtered plasma is shown. Fraction 26 proved positive for HBV-DNA and HBsAg. (E) HBV virions
824 contained in high density fraction 3 were further purified by CsCl-density centrifugation. After
825 buffer-exchange to PBS, HBV virions were incubated for 30 minutes at 37°C with or without
826 human serum (10% v/v; anti-HBs-negative) and subjected to sucrose density gradient
827 centrifugation. HBV-DNA was detected in fractions of low density (indicated by arrows) after
828 incubation with serum (lower row). (F) Mixed ELISA of human plasma containing HBV (left
829 panel: 3×10^5 - 3×10^7 virions; right panel: 3×10^5 virions) using anti-ApoB (left panel) or anti-
830 ApoE capture (right panel) and anti-HBs detection antibodies. (G) Proteins detected by mass
831 spectrometry of supernatant-purified HBV subviral particles (HepG2-LMS) or control fractions
832 show association of ApoE and HBsAg (red cross). (H) HBV particles purified by sucrose
833 density ultracentrifugation from stable producer cells HepAD38 were analysed by immune
834 electron microscopy with gold-labelled anti-ApoE- (upper panel) and anti-HBsAg-specific
835 antibodies (picture below). Pictures show distant localisation of ApoE and proximal localisation
836 of HBsAg. Scale bars indicate 50 nm.

837

838 **Figure 6: Functional role of the association of HBV with lipoproteins**

839 (A) HepG2-NTCP cells were infected with high pure luciferase expressing recombinant HBV
840 in the presence or absence of FCS (left) or in the presence of serum from ApoE KO or control
841 mice (right). On day seven cell culture supernatants were analysed for luminescence
842 intensities. (B) Differentiated HepaRG-cells were incubated with an LDL-receptor blocking
843 antibody (anti-LDL-R) either before or before and during HBV infection or four days after
844 infection. On day 12 post HBV infection HBeAg was determined in the cell supernatant by
845 ELISA and cccDNA was quantified in cell lysates by quantitative RT-PCR. (C-E) Isolated liver
846 macrophages were incubated for 1h with VP₅₉₄ in medium containing 10% human serum and
847 washed. In (C) 5 µg/ml chylomicron NBD-cholesterol was added for 2 hours, in (D) 2 µg/ml
848 HDL₄₈₈ was added for 1h before fixation. (E) Cells were fixed and stained for ApoA1. Merged
849 pictures show VP₅₉₄ in red, NBD-cholesterol, HDL₄₈₈, and ApoA1 staining in green, and nuclear
850 staining with DAPI in blue. Scale bars indicate 1 µM **p<0.01; ***p<0.001; ****p<0.0001.

851

852 **Fig 7: Recycling of HBV along intracellular transport pathways of free cholesterol.**

853 (A-C) Monocyte derived macrophages were loaded for 16h with cholesterol using medium
854 containing 50 µg/ml acLDL, incubated with VP₅₉₄ containing medium for 1h and further
855 incubated for 4h with acLDL containing medium without VP₅₉₄. After fixation cells were stained
856 with filipin to detect free cholesterol. (A) Total cellular (total) and perinuclear (pn) areas of a
857 representative cell are indicated by dashed lines. The boxed area is exemplarily shown
858 enlarged below the main panels separately for each channel. Merged pictures show VP₅₉₄ in
859 red and filipin staining in green. Scale bar is 10 µm. (B, C) 5 µM U18666A was added to the
860 culture medium as indicated. (B) Representative vision fields of several macrophages. (C)
861 Relative fluorescence intensity (I) of filipin- and Alexa 594® in the cell periphery were calculated
862 by subtracting pn from total signals and multiplying these with the corresponding area to
863 quantify the content of free cholesterol and VP₅₉₄. The diagram gives the ratio of pn to
864 peripheral cholesterol (Filipin, dots) and VP₅₉₄ (triangles) in analysed cells. Scale bar is 10 µm
865 (A) or 100 µm (B). (D-E) THP macrophages were incubated with HBV in serum free medium
866 for 3h, washed and further cultured for 16h with 0,2% BSA containing medium only or medium
867 supplemented with 100 or 200 µg/ml HDL as indicated. (D) Supernatants of macrophages
868 were collected and analysed for HBsAg or (E) HBV-DNA content. (F) THP macrophages were
869 incubated with HBV in 0,2% BSA containing medium for 3h, washed and further cultured for

870 16h with 0,2% BSA containing medium only or supplemented with 25 µg/ml ApoA1. (G) THP
871 cells were incubated with HBV and 1 µg/ml [3H]-cholesterol-chylomicrons in serum free
872 medium (w/o) or medium containing 10% human serum. Cells incubated with neither HBV nor
873 [3H]-cholesterol-chylomicrons were used as negative control (-). In cell lysates and
874 supernatant, HBV-DNA was quantified by real time PCR, and [3H]-cholesterol content was
875 determined by liquid scintillation counting. Mean values ± SD of four independent experiments
876 are given.

877

878 **Fig 8: HBV transport from liver macrophages into hepatocytes.**

879 (A-E) Human liver tissue was perfused with medium containing VP₅₉₄ (shown in red) and 50%
880 human serum for 1h, followed by a 16h perfusion without HBV before fixation. DAPI staining
881 is shown in blue. All scale bars are 10 µm. (A) Immunofluorescence staining for CD68+ liver
882 macrophages. The tissue shows liver sinuses with hepatocytes neighbored by several
883 CD68+-stained liver macrophages. The boxed area is shown as enlargement below the main
884 panels separately for each channel and focuses on one liver macrophage located in a liver
885 sinus next to two hepatocytes. The dotted line indicates the circumference of one hepatocyte
886 next to the macrophage. (B) Localization of HBV particles within one exemplary HepPar1+
887 hepatocyte (green). Z-axis projections are given for each channel. (C) Quantification of HBV-
888 positive CD68+ liver macrophages, CD68- cells and HepaPar1+ hepatocytes in ten random
889 vision fields at 200-fold magnification. Mean values ± SD. (D, E) Staining of neutral lipids with
890 BODIPY493/503 shown in green within (D) a liver sinus with hepatocytes neighbored by two
891 liver macrophages or (E) focussing one hepatocyte and one liver macrophage indicated by
892 (Hep) and (KC), respectively. Hepatocytes (Hep) and liver macrophages (KC) are indicated.
893 (D) shows xy images at two different z-positions of the same vision field. (E) Boxed areas are
894 shown as enlargements for different z positions on the right. (F) Staining for SR-B1 (shown in
895 green). The arrow indicates VP₅₉₄ localised to SR-B1 positive plasma membranes. The area
896 highlighted by the white box is enlarged on the right. (G) Relative localization of VP₅₉₄ and
897 CD68-positive liver macrophages (green) after 1h (left picture) and 17h perfusion (right
898 picture). For increased contrast, DAPI staining is shown in white. Hep: hepatocyte. All scale
899 bars are 10 µm.

900

901 **Fig 9: Trans-infection of hepatocytes by HBV taken up by liver macrophages.**

902 Primary liver macrophages (KC) and hepatocytes (PHH) were isolated from the same donors.
903 (A) KC were loaded with VP₅₉₄ for 4h, thoroughly washed and co-cultured with hepatocytes
904 pre-labelled with 5-chloromethyl-fluorescein diacetate (CMFDA, green). One representative
905 hepatocyte and liver macrophage each is shown. Lower panel shows Z-axis projection at the
906 dashed line. (B) Macrophage / hepatocyte mix culture was incubated with 2 µg/ml Alexa Fluor
907 488®-labelled acLDL (green) for 6h to stain macrophages. acLDL staining (left), phase contrast
908 (middle) and overlay (right) are shown. The arrow indicates a membrane connection between
909 a macrophage and a hepatocyte. (C) Freshly isolated hepatocytes were incubated with 5 µM
910 Dil for 20 min, washed three times by centrifugation at 300g and seeded onto a culture of liver
911 macrophages from the same donor for 16h. A close connection that has established between
912 a hepatocyte and a macrophage is shown. The area highlighted by the white box is shown
913 enlarged below. Background fluorescence was acquired in a far-red fluorescence channel.
914 Merged pictures (right panel) show Dil in red and nuclear staining with DAPI in blue. (D)
915 Isolated KC were incubated with HBV for 6h at either 4°C or 37°C as indicated and washed,
916 trypsinized, seeded and washed again before added to PHH. Widefield microscopy of

917 macrophage / hepatocyte mix cultures (left and middle panel) and pure liver macrophages
918 (right panel) at day 12 post infection. **(E-G)** Liver macrophages (KC) were incubated with HBV
919 for 6h at 4°C (dark gray bars) or 37°C (light grey bars) and washed, trypsinized, seeded and
920 washed again before hepatocytes (PHH) were added. **(E)** Detection of HBV cccDNA in cell
921 lysates. **(F)** HBsAg and HBeAg were measured in co-culture media. **(G)** Negative control with
922 KC only. Values are mean ± SEM of two independent experiments, triplicates each. **(H, J)**
923 Primary macrophages were incubated with HBV in the presence or absence of 100 µM
924 Bulevertide or ant-HBsAg-antibodies (H) or with 5 µM U18666a (J), washed, trypsinized,
925 seeded and washed again before hepatocytes (PHH) were added. On day 12, HBV RNAs (H)
926 or HBV cccDNA (J) were quantified. Values are mean ± SD (H) and ± SEM (J) of two (H) and
927 three (J) independent experiments, triplicates each. **(I)** Primary human hepatocytes only (left
928 panel) or primary human macrophages (right panel) were incubated with 1×10^8 /ml virions.
929 Then, cells were either washed (hepatocytes only culture) or trypsinized and thoroughly
930 washed before hepatocytes were added to macrophages. On day 12 post infection, HBV
931 cccDNA was quantified in cell lysates. Values are mean ± SEM of three independent
932 experiments, quadruplicates each. **p < 0.01, ***p < 0.001 and ****p < 0.0001. Scale bars are
933 10 µm **(A-C)** or 100 µm **(D)**.

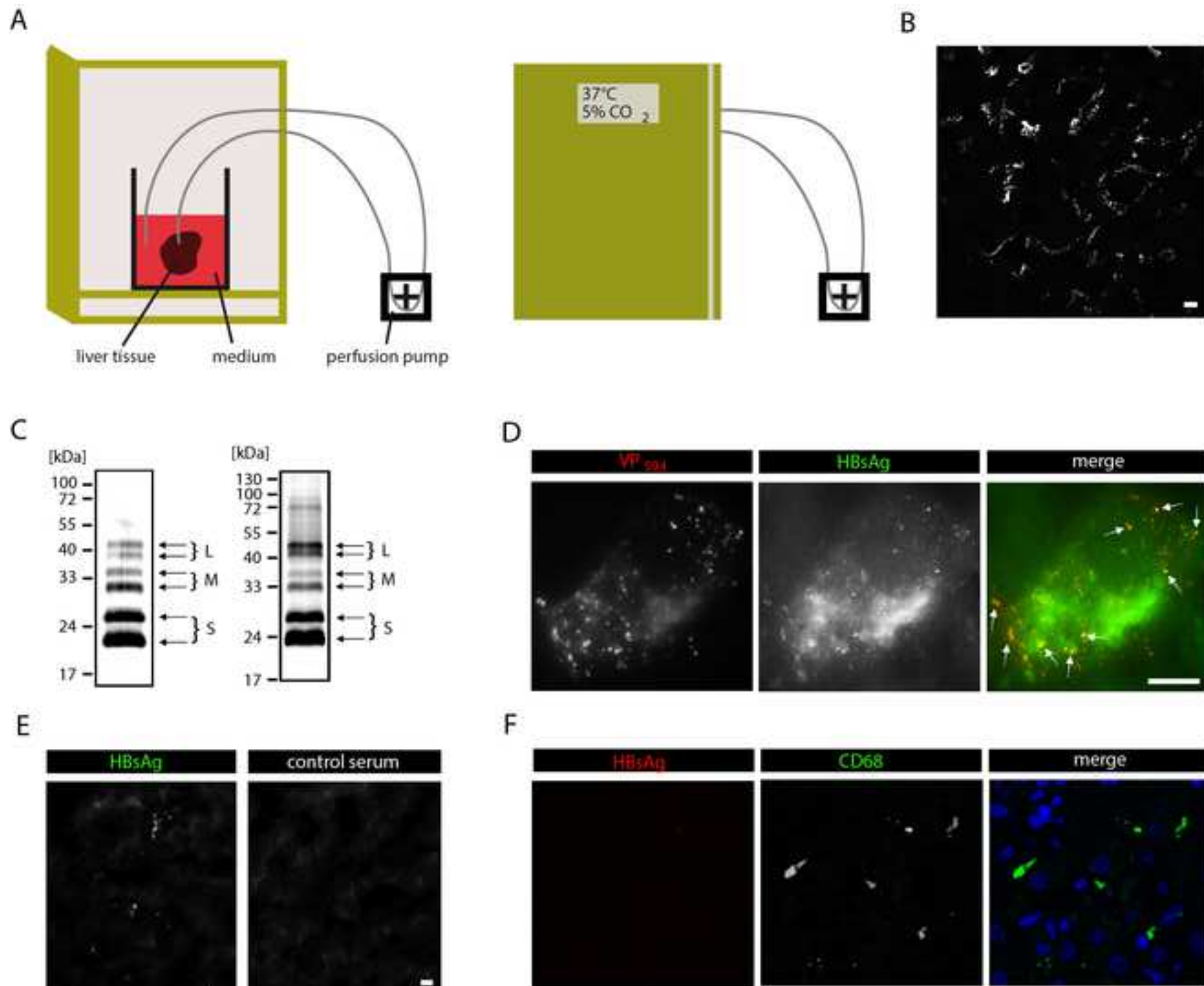
934

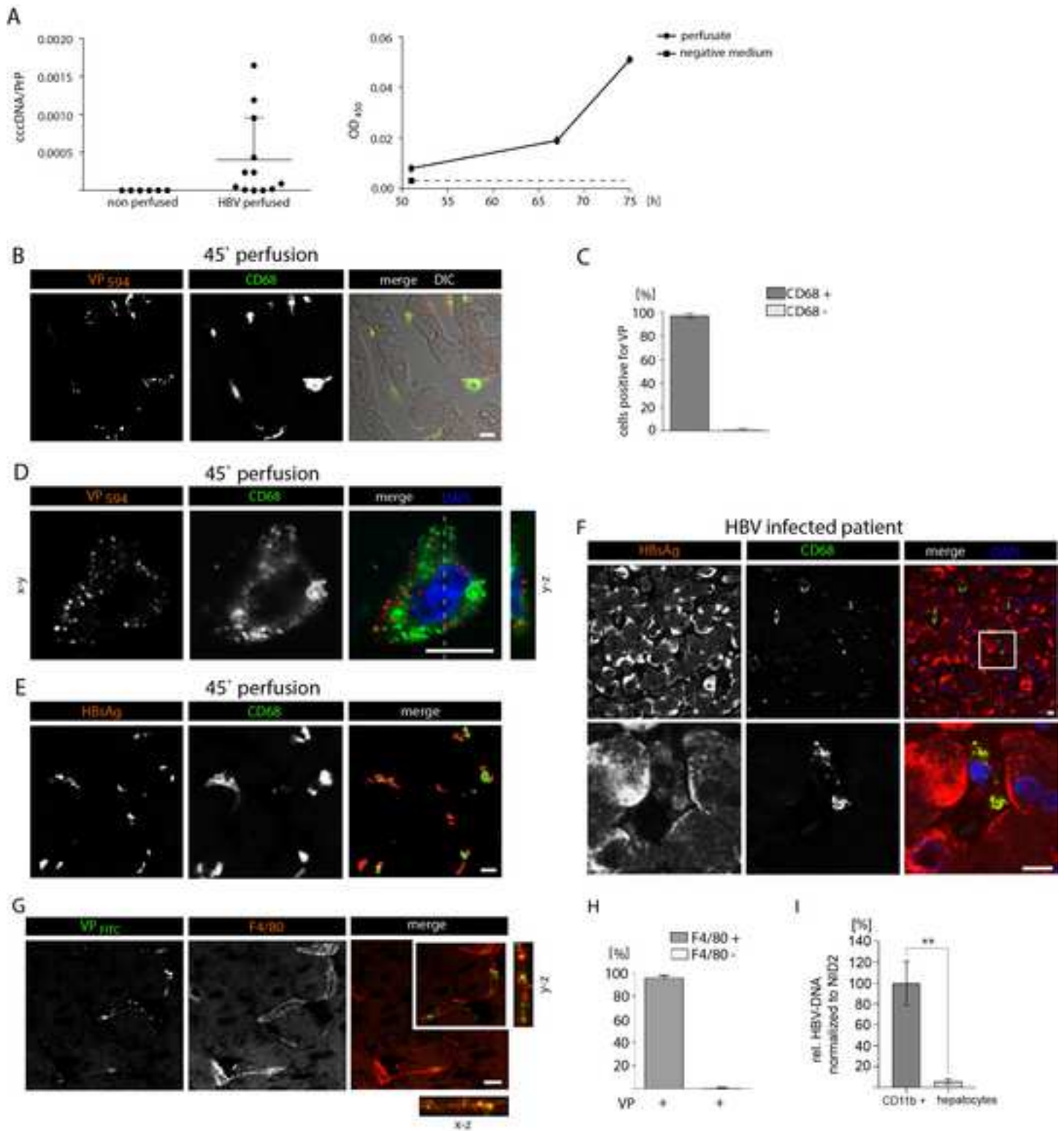
935

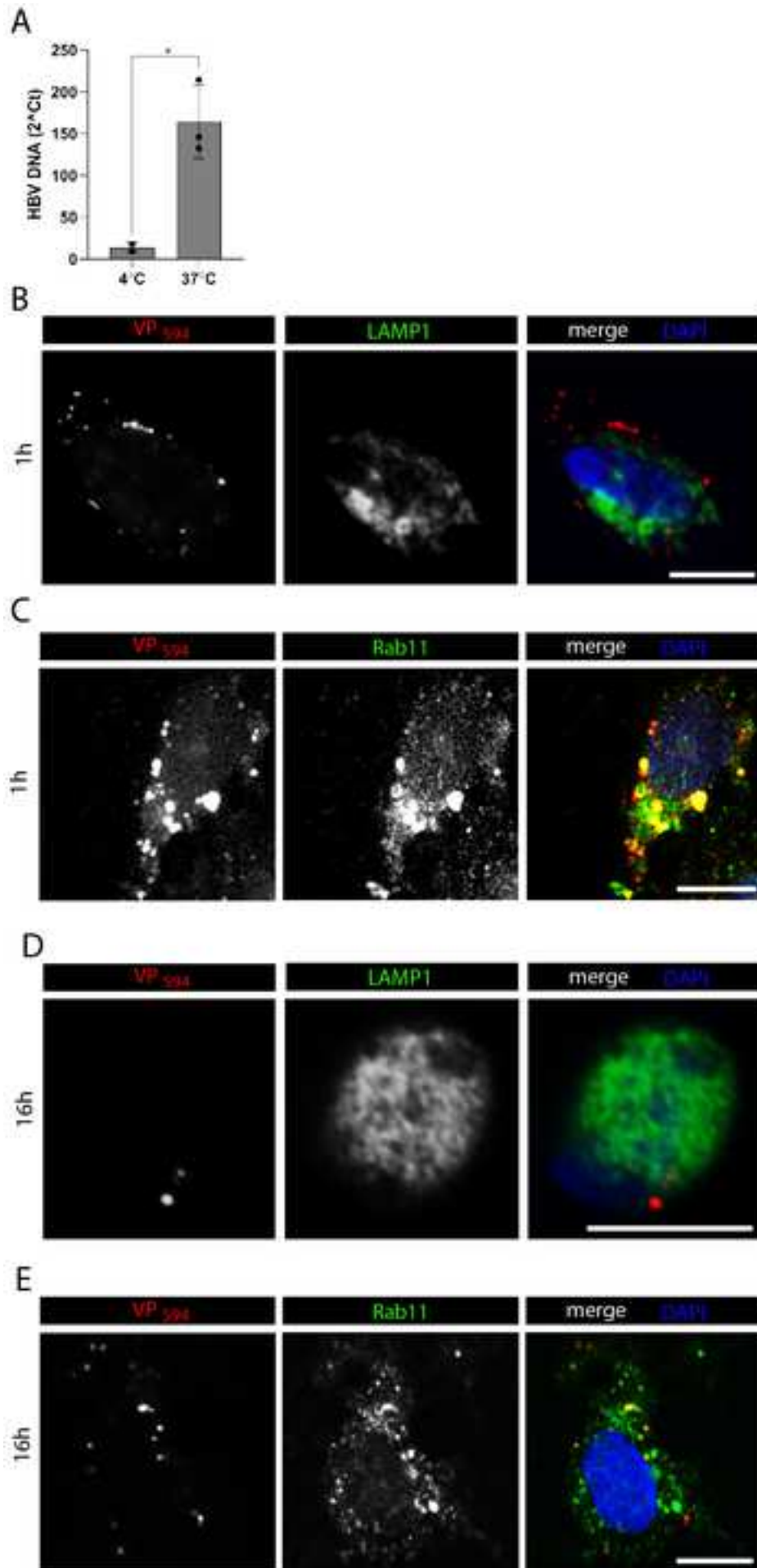
936

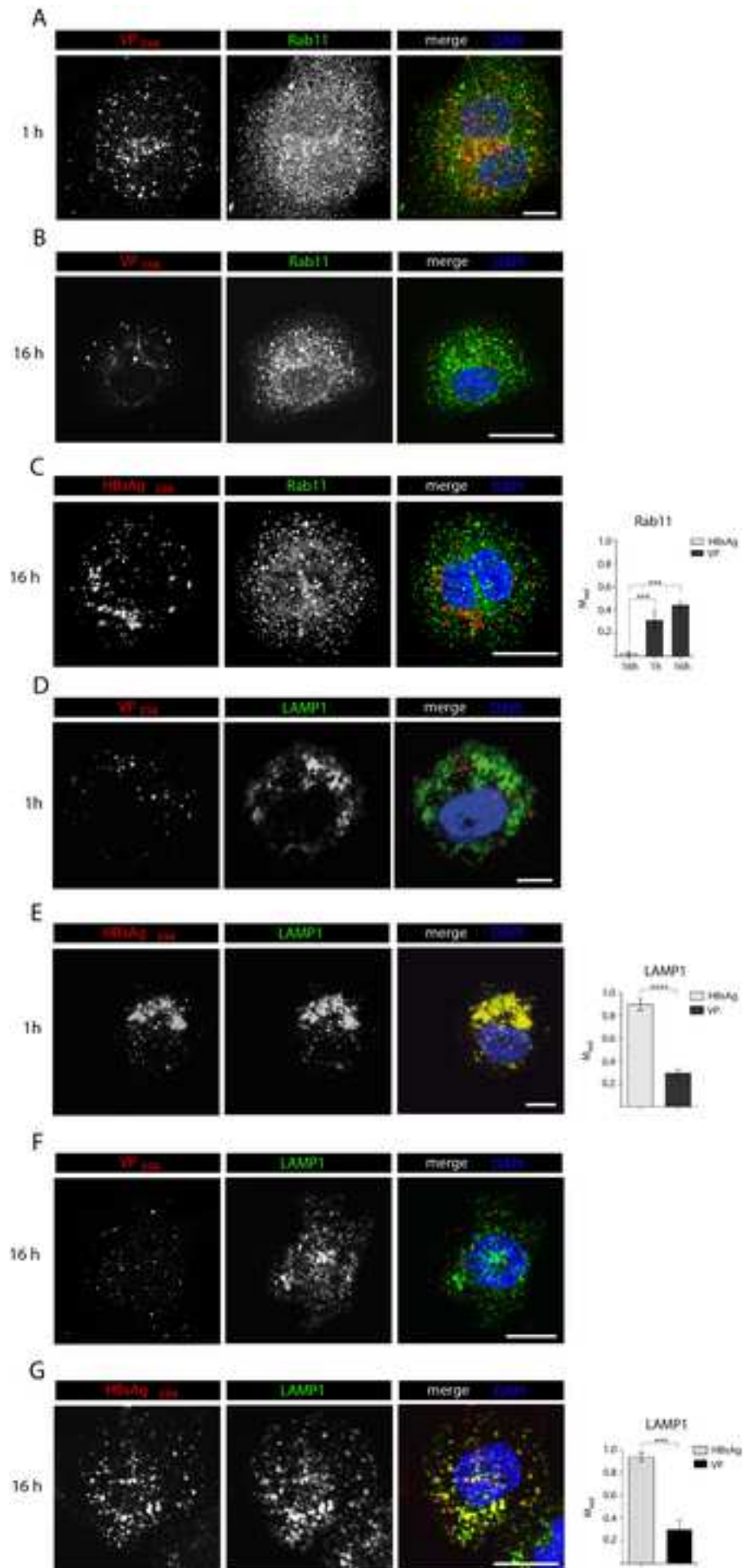
937

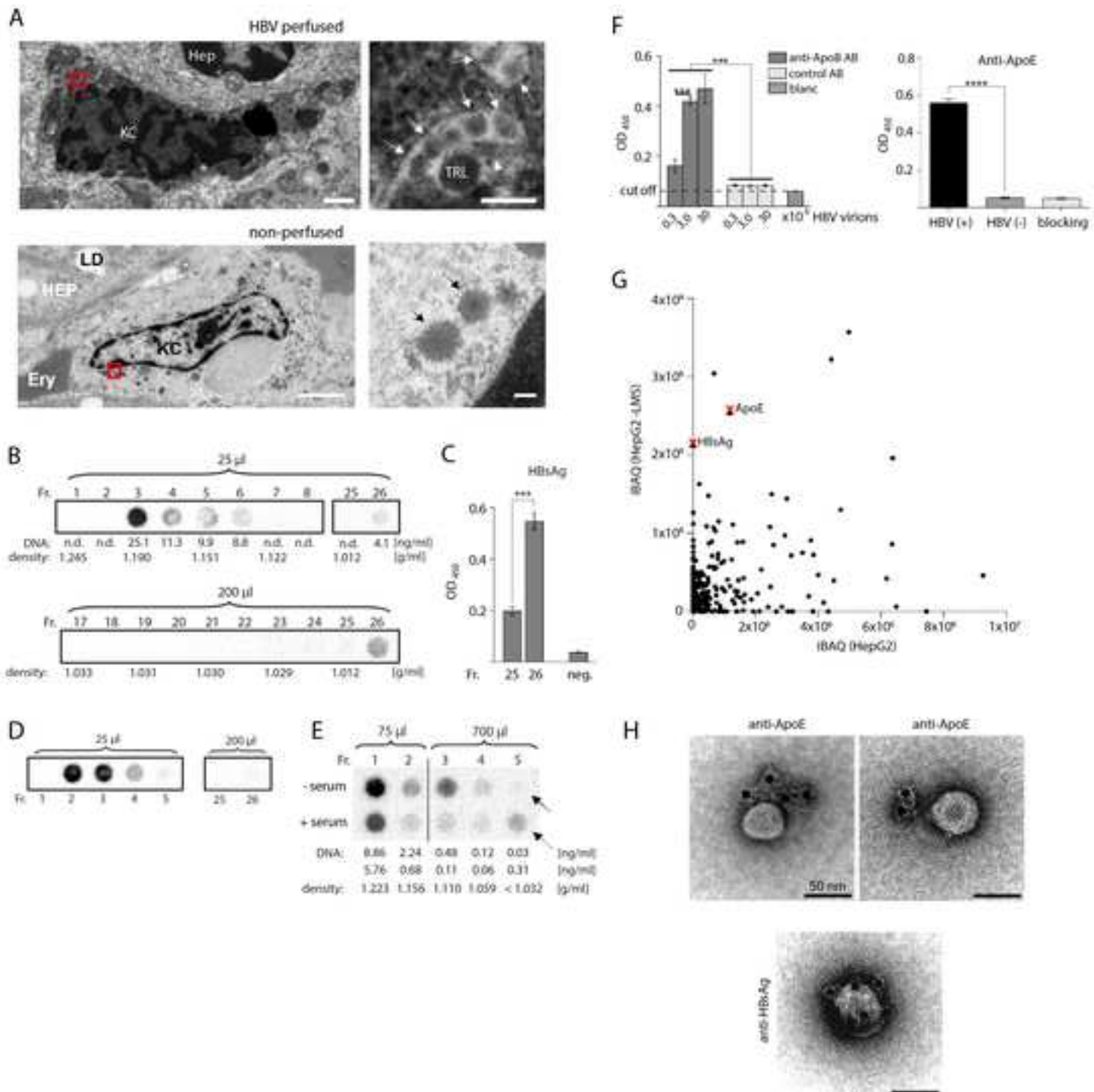
938 **Supporting Information (text file): EXTENDED EXPERIMENTAL PROCEDURES**

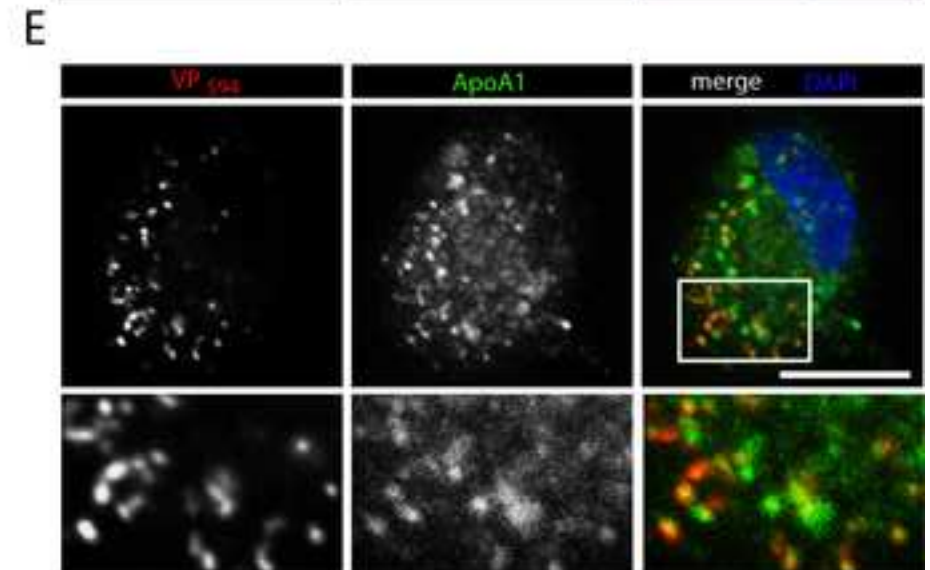
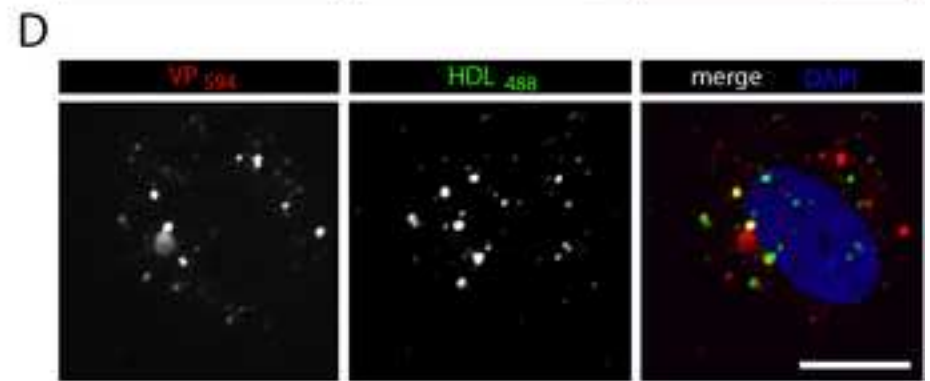
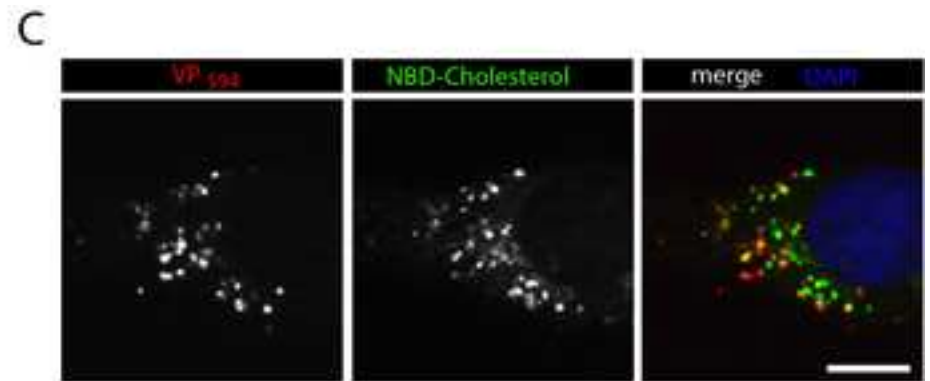
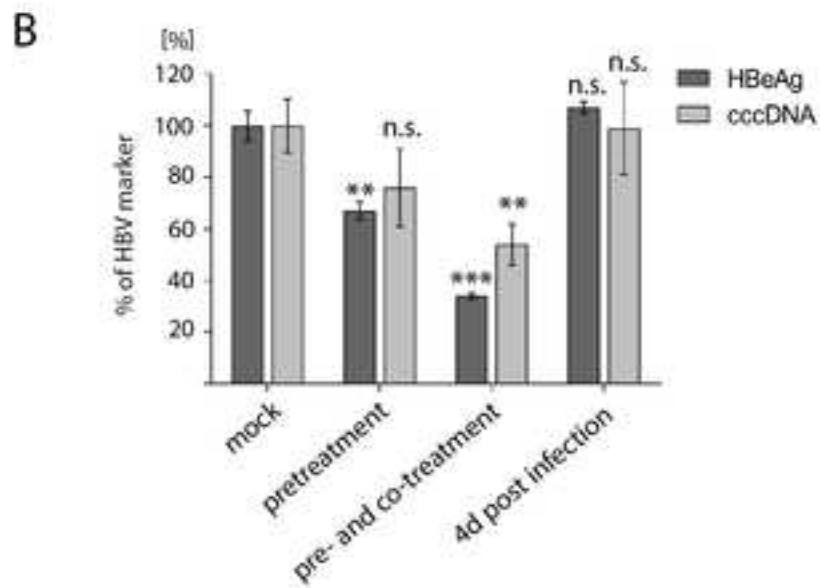
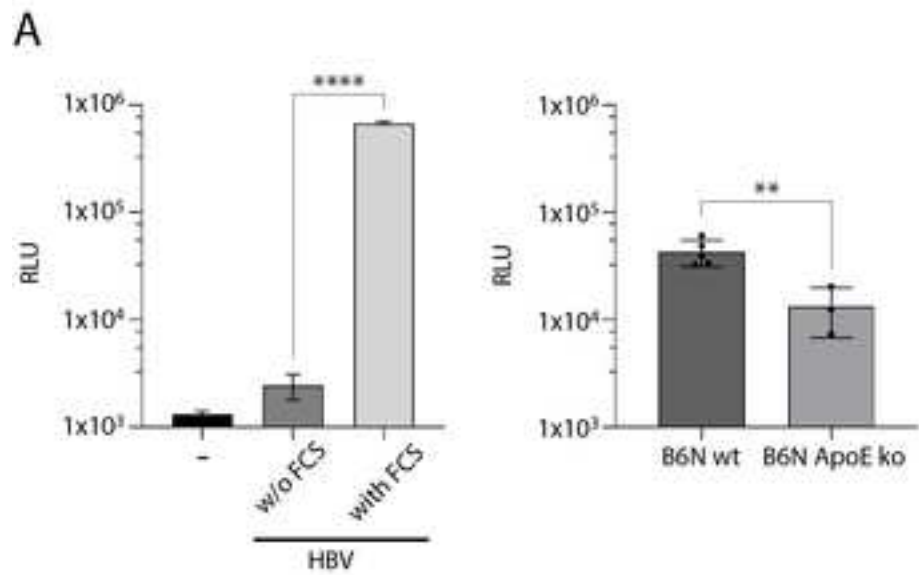


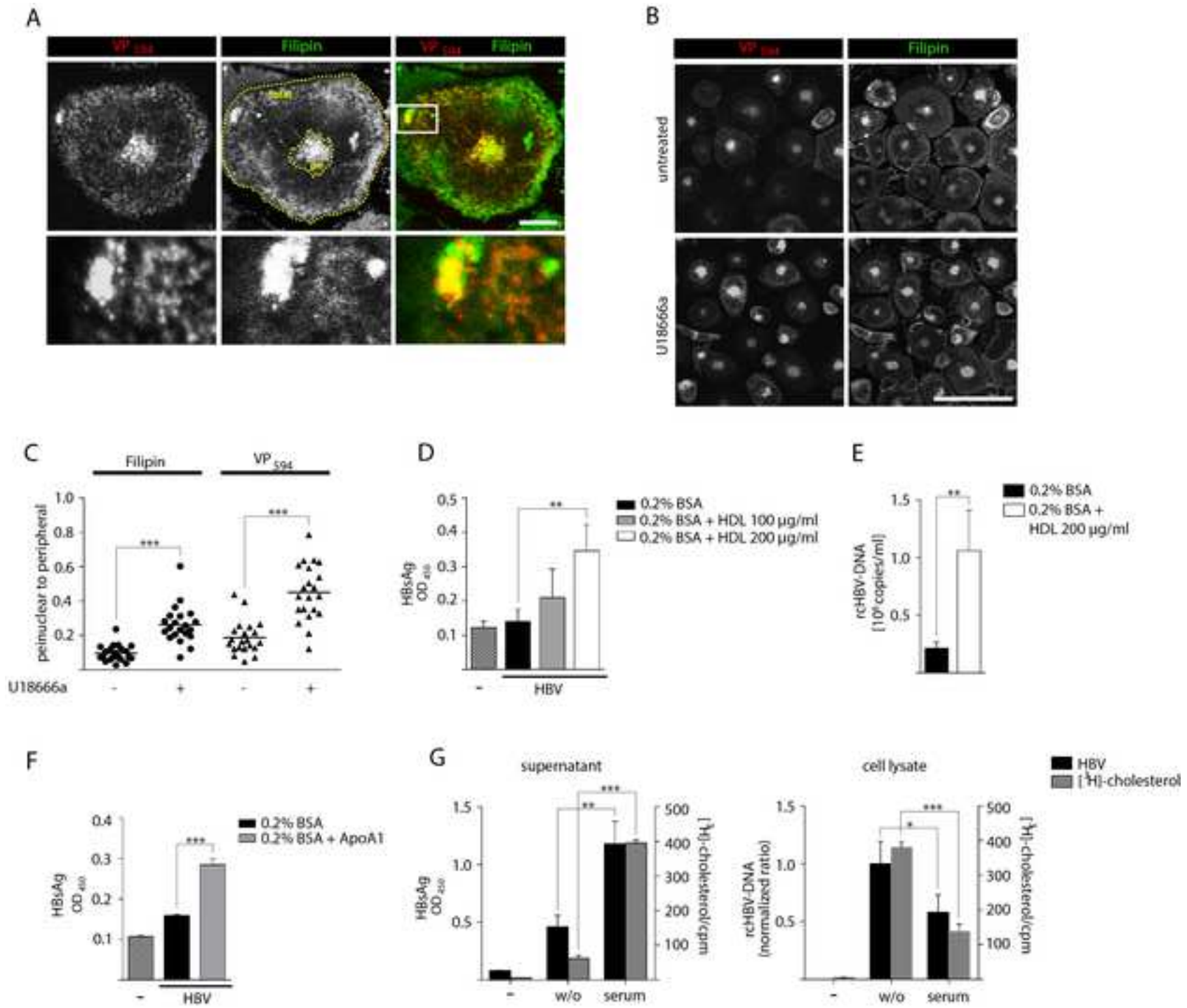


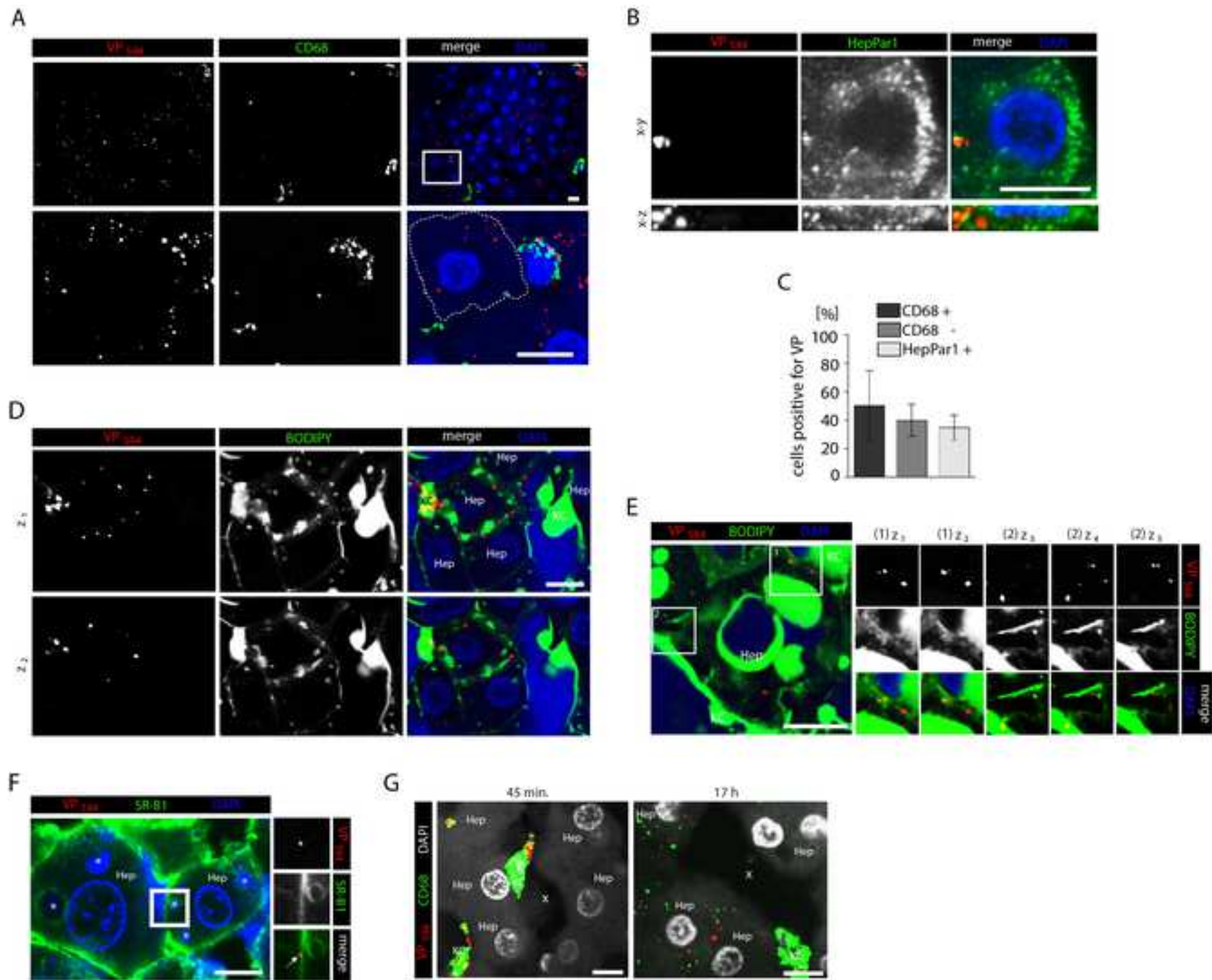


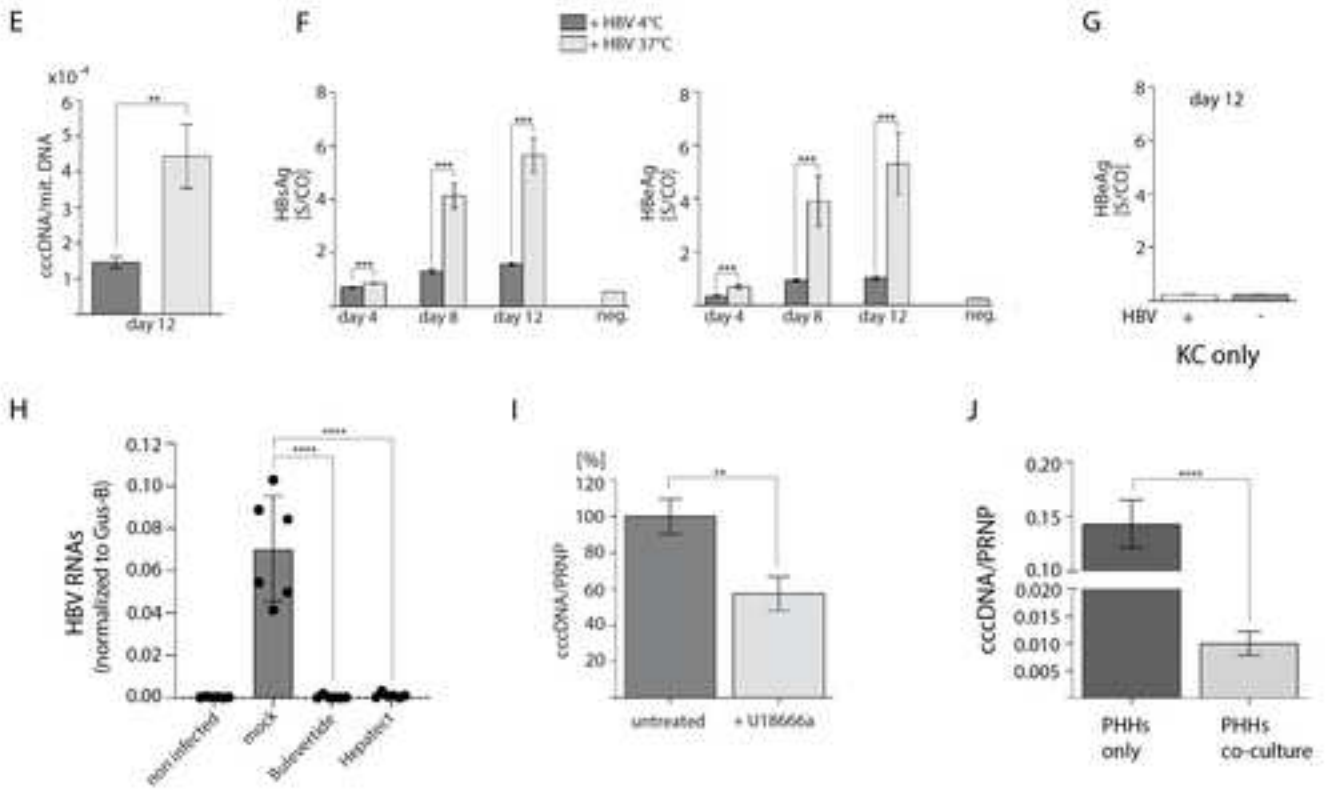
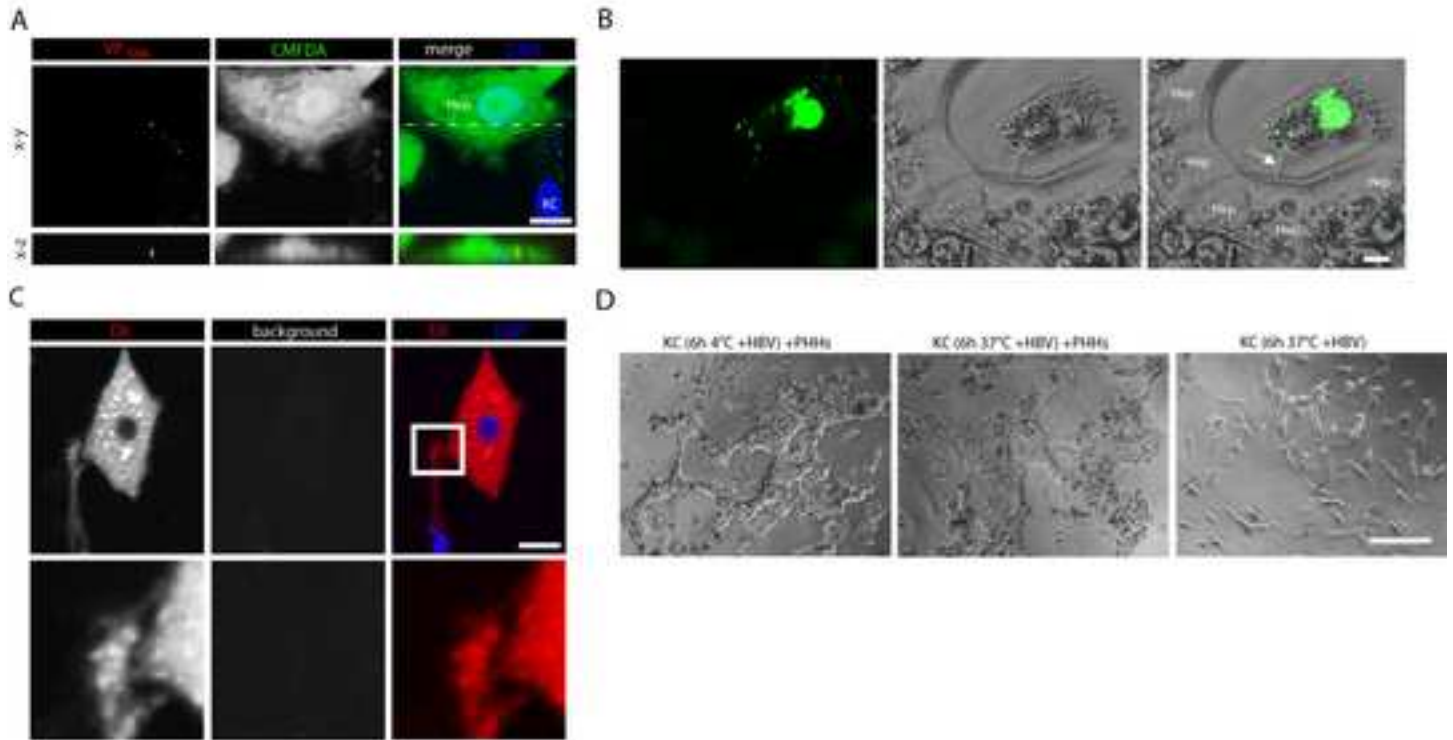












Revised Manuscript in Word or RTF (no changes marked)

[Click here to view linked References](#)



Click here to access/download

Revised Manuscript in Word or RTF (no changes marked)

Esser, Cheng, Wettengel et al., 2023.docx



Click here to access/download

Supplemental material (large tables and data sets only)

Supporting information_extended experimental
procedures.doc

